



Chem Soc Rev

**Taming excited state reactivity of Imines – From non-radiative decay to Aza Paternò-Büchi reaction**

Journal:	<i>Chemical Society Reviews</i>
Manuscript ID	CS-SYN-06-2020-000717.R2
Article Type:	Review Article
Date Submitted by the Author:	26-Oct-2020
Complete List of Authors:	Kandappa, Sunil; Bowling Green State University, Chemistry Valloli, Lakshmy; Bowling Green State University, Chemistry Ahuja, Sapna; Bowling Green State University, Chemistry Parthiban, Jayachandran; Bowling Green State University, Chemistry Sivaguru, Jayaraman; Bowling Green State University, Chemistry

SCHOLARONE™  
Manuscripts

## ARTICLE

# Taming excited state reactivity of Imines – From non-radiative decay to Aza Paternò-Büchi reaction

Received 00th January 20xx,  
Accepted 00th January 20xx

DOI: 10.1039/x0xx00000x

Sunil Kumar Kandappa,<sup>a</sup> Lakshmy Kannadi Valloli,<sup>a</sup> Sapna Ahuja,<sup>a</sup> Jayachandran Parthiban,<sup>a</sup> J. Sivaguru\*<sup>a</sup>

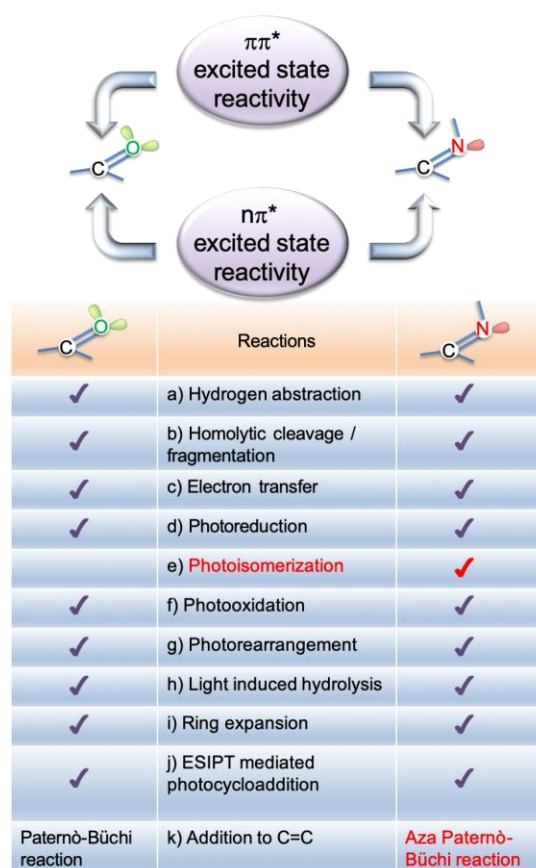
**Abstract:** The review highlights the excited state characteristics of imines and processes that govern its photochemical and photophysical properties. The review examines pathways for deactivation and the type of photochemical reactions that originates from excited imines. The review also features recent strategies that are developed to circumvent the fundamental issues that have plagued the development of the Aza Paternò-Büchi reaction.

## 1. Introduction

Imines continue to play a seminal role in the development of organic ground state reactions.<sup>1–3</sup> The excited state characteristics of imines have placed significant hurdles for enhancing the scope of the photochemical reactions involving C-N double bonds.<sup>4,5</sup> This becomes quite clear when one compares the exhaustive photochemistry that has been developed for imine's close cousin, the carbonyl functionality (Figure 1).<sup>6</sup> One of the fundamental issues that curtailed the development of photochemical reactions involving imines compared to their carbonyl counterparts is the poor appreciation of the excited state reactivity of C-N double bond. This review highlights the relaxation / reaction pathways that are typically encountered upon photoexcitation of imines, the type of photoreactions that are expected based on the excited state nature of imines and how one can develop new excited state photochemical reactivity involving C-N double bond.

### 1.1 Scope of this review

An overview of the literature reveals that there are few reviews related to the photochemistry of imines. The earliest review to highlight the complexities of imines was detailed independently by Padwa<sup>4</sup> and Pratt<sup>5</sup> in 1977. Recent reviews have highlighted the synthetic utility of imines for accessing azetidines<sup>7</sup> and utilizing imines in photoredox chemistry.<sup>8</sup> This review aims to fill the void in the chemical literature by



	Reactions	
✓	a) Hydrogen abstraction	✓
✓	b) Homolytic cleavage / fragmentation	✓
✓	c) Electron transfer	✓
✓	d) Photoreduction	✓
	e) Photoisomerization	✓
✓	f) Photooxidation	✓
✓	g) Photorearrangement	✓
✓	h) Light induced hydrolysis	✓
✓	i) Ring expansion	✓
✓	j) ESIPT mediated photocycloaddition	✓
Paternò-Büchi reaction	k) Addition to C=C	Aza Paternò-Büchi reaction

**Figure 1.** Comparison of excited state reactivity of carbonyl and imine functionalities.

surveying the excited state characteristics of imines, the processes that govern the both photochemical and photophysical events. In addition, the review also highlights the photochemical reactivity of chromophores featuring C=N

<sup>a</sup> Center for Photochemical Science and Department of Chemistry, Bowling Green State University, Bowling Green, Ohio 43403, USA

<sup>b</sup> E-mail: sivagj@bgsu.edu

<sup>†</sup> SK current address: Dept of Chemistry, University of Southern California, USA. SA current address: Dept of Biochemistry and Biophysics, University of Pennsylvania, USA

double bonds such as oxadiazoles, isoxazolines or acyclic oximes to broaden the coverage of “imine” photochemistry. For photochemistry of iminium ions readers are encouraged to recent literature reviews on topic.<sup>9</sup> The review highlights selected examples in each of the category to highlight readers about the complexities involved in excited state reactivity of imines. These will help chemists to develop new strategies for controlling different photochemical reactivity of imines and its derivatives.

## 2.0 Ground and Excited state characteristics of imines

### 2.1 Spectroscopic features of imines

The electronic absorption characteristics of imines  $R_2C=NR$  are similar to carbonyl compounds and feature an intense  $\pi\pi^*$  absorption and very weak  $n\pi^*$  absorption band.<sup>10</sup> Oftentimes, the forbidden  $n\pi^*$  transition is weak and occurs at a lower energy when compared to the allowed  $\pi\pi^*$  transition that is typically observed at higher energies. These absorptions often overlap with the  $n\pi^*$  transitions presenting itself as a shoulder (at lower energy) adjacent to intense  $\pi\pi^*$  absorption. An empirical way to distinguish between the two is by observing the solvent effect on UV-Vis spectra of a molecule.<sup>11,12</sup> In this regard, Bonnett and co-workers<sup>13</sup> performed the solvent studies on absorption characteristics of various substituted pyrrolines **1a-f** (Figure 2; refer cyclic imines) and attributed the long wavelength absorption to  $n\pi^*$  transition of C=N bond. This long wavelength absorption in pyrrolines **1a-f** featured a low extinction coefficient ( $\epsilon$ ) and displayed blue shifted absorptions when the solvent was changed from non-polar hexane to polar protic ethanol.<sup>13</sup> For example, 2-methyl-1-pyrroline **1a** showed an  $n\pi^*$  absorption centered at 227 nm in hexanes with a molar absorptivity ( $\epsilon$ ) of  $214\text{ M}^{-1}\text{ cm}^{-1}$ , while in ethanol the  $n\pi^*$  absorption centred around 216 nm i.e., a hypsochromic shift of 10 nm, with a molar absorptivity  $199\text{ M}^{-1}\text{ cm}^{-1}$ .<sup>13</sup> Extending the conjugation in cyclic imines by aryl substitution on the imine carbon led to an enhancement of absorptivity at longer wavelengths. For example, the molar absorptivity of 3,3-dimethyl-2-phenyl-1-pyrroline **1f** ( $8912\text{ M}^{-1}\text{ cm}^{-1}$ ) is about 53 times the molar absorptivity of 3,3-dimethyl-2-isopropyl-1-pyrroline **1d** ( $166\text{ M}^{-1}\text{ cm}^{-1}$ ) in ethanol. This was attributed to the possible mixing of  $n\pi^*$  and  $\pi\pi^*$  states in the aryl conjugated system 3,3-dimethyl-2-phenyl-1-pyrroline **1f**. The long wavelength  $n\pi^*$  absorption band was also susceptible to protonation that resulted in its disappearance in acidic media due to binding of  $n$  electrons with a concurrent bathochromic shift of the intense  $\pi\pi^*$  absorption of protonated imine ( $R_2C=NRH^+$ ). For example, 3,3-dimethyl-2-phenyl-1-pyrroline **1f** showed an  $n\pi^*$  absorption that overlapped with an  $\pi\pi^*$  absorption centered at 239 nm in ethanol with a molar absorptivity of  $8912\text{ M}^{-1}\text{ cm}^{-1}$ , that upon protonation in ethanol leads to disappearance of  $n\pi^*$  absorption band at 239 nm with simultaneous appearance of  $\pi\pi^*$  band at 267 nm.

Nelson and co-workers also investigated the solvent dependent behaviour of UV-Vis spectra of alkyl imines **2a-f**

(Figure 2; refer acyclic imines).<sup>14</sup> Analysis of UV-Vis spectra of imines indicated that the absorption band around 180 nm corresponds to  $\pi\pi^*$  absorption owing to higher extinction coefficient lying in range between  $5000\text{--}10000\text{ M}^{-1}\text{ cm}^{-1}$ . The  $n\pi^*$  absorption was characterized by the lower extinction coefficient  $\epsilon$  lying in range between  $140\text{--}290\text{ M}^{-1}\text{ cm}^{-1}$ . Additional evidence was provided by the blue shifted  $n\pi^*$  band in polar solvent ethanol as compared to non-polar solvents. For example, N-isopropylideneimine **2a** featured  $\pi\pi^*$  absorption band centered at 181 nm with molar absorptivity ( $\epsilon$ ) of  $5980\text{ M}^{-1}\text{ cm}^{-1}$  in n-heptane and  $n\pi^*$  band at 244 nm with molar absorptivity ( $\epsilon$ ) of  $160\text{ M}^{-1}\text{ cm}^{-1}$  in cyclohexane. The  $n\pi^*$  band underwent a hypsochromic shift to 231 nm in EtOH while the molar absorptivity ( $\epsilon = 160\text{ M}^{-1}\text{ cm}^{-1}$ ) remained same. Similarly, imine **2e** that featured an exo-double bond was characterized by a  $\pi\pi^*$  absorption band centered at 181 nm with molar absorptivity ( $\epsilon$ ) of  $9275\text{ M}^{-1}\text{ cm}^{-1}$  and  $n\pi^*$  band at 250 nm with molar absorptivity ( $\epsilon$ ) of  $246\text{ M}^{-1}\text{ cm}^{-1}$ . A hypsochromic shift to 240 nm in EtOH was observed for  $n\pi^*$  band in **2e**.

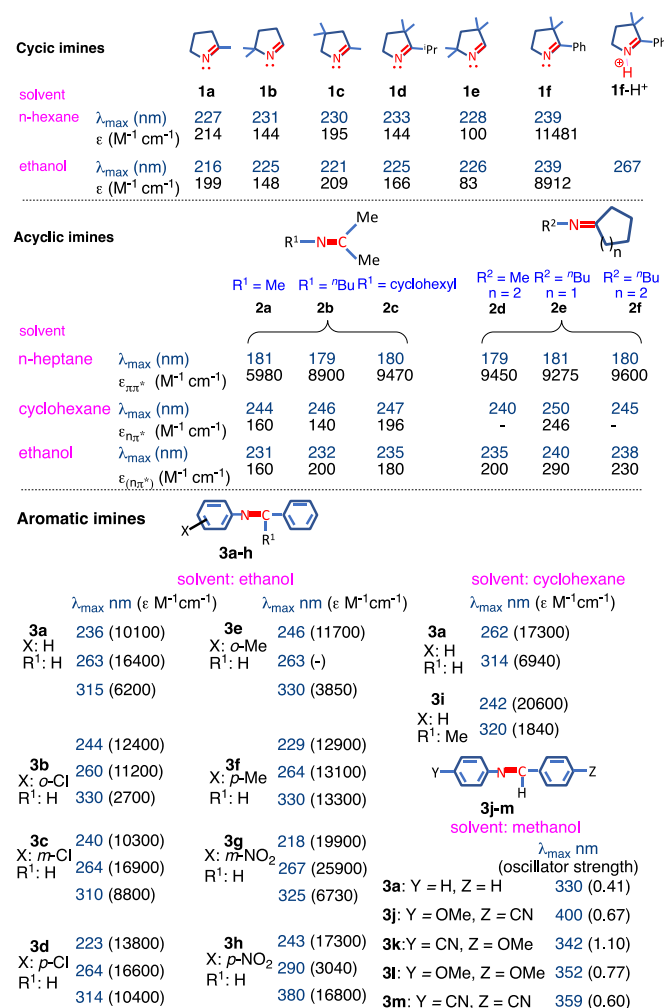


Figure 2. Ground state absorption characteristics of selected cyclic imines **1a-f** and acyclic imines **2a-f** and **3a-h**.

Ebara and co-workers<sup>15</sup> studied the UV-Vis behaviour of substituted aromatic imines **3a-h** (Figure 2; refer aromatic

imines). One of the features in aromatic imines is the extension of conjugation that makes the imine-double bond as part of an extended  $\pi$ -system. This extended conjugation caused a bathochromic shift of absorptivity in aromatic imines. The extension of conjugation also caused the mixing of the  $n\pi^*$  and  $\pi\pi^*$  states that was reflected in the molar absorptivity. For example, comparing the  $n\pi^*$  absorption in acyclic imines **2a-f** and aromatic imines **3a-h** in EtOH indicated that  $n\pi^*$  bands in aromatic imines **3a-h** are red shifted by at least 50 nm compared to that in acyclic imines **2a-f**. High molar absorptivities of the absorption bands lying in range between 315–380 nm in **3a-h** indicated the possible mixing of  $n\pi^*$  and  $\pi\pi^*$  states.

Spectral properties of simple aromatic imine like benzylidene imine **3a** (Figure 2) has been studied by various researchers.<sup>14,16–19</sup> Jaffé and co-workers<sup>16</sup> suggested that the band at 263 nm arises from  $\sigma\pi^*$  transition and band at 315 nm arise due to  $\pi\pi^*$  transition. They proposed that  $n\pi^*$  transition was around 360 nm as an overlapping shoulder of the  $\pi\pi^*$  transition (due to its low  $\epsilon$  of  $\sim 100 \text{ M}^{-1}\text{cm}^{-1}$ ). Mehlhorn and co-workers suggested the possibility of mixing of  $\pi\pi^*$  and  $n\pi^*$  transition.<sup>17</sup> The mixing of states was attributed to the non-planarity of imine **3a** as the angle of distortion was found between  $52^\circ - 55.2^\circ$  established by X-ray analysis and electron diffraction. The research groups of Smith<sup>18</sup> and Bentrup<sup>19</sup> independently investigated the effect of substituent on  $\alpha$ -hydrogen of imine by comparing spectral properties of imine **3a** and **3i**. It was inferred from the UV-Vis data of imines that the presence of an  $\alpha$ -substituent, for example, methyl group contributed to the non-planarity of imine due to increased torsional angle between the phenyl groups of C=N bond in imine. This was reflected in the intensities of  $\pi\pi^*$  band at 314 nm (for **3a**) and 320 nm (for **3i**). Additionally, short wavelength transition was red shifted in **3i** (320 nm) compared to **3a** (314 nm) while the long wavelength transition was blue shifted in **3i** (242 nm) compared to **3a** (262 nm) in cyclohexane.

The spectral properties of imines was evaluated by Luo and co-workers that gave further insight into the substituent effect on imines.<sup>20</sup> The presence of  $\pi$ -donor and  $\pi$ -acceptor groups and their relative position in imines exerts a major effect on the  $\pi\pi^*$  absorption characteristics. For example, comparing the wavelength of lowest energy absorption in **3a**, **3j** and **3k** (Figure 2) indicates that red shift is observed in methoxy (**3j**) and cyano (**3k**) substituted aromatic imine compared to unsubstituted imine **3a**.<sup>20</sup> The bathochromic shift was more pronounced in the imine that featured a push-pull system (compare **3j** with **3m**) where  $\pi$ -donating OMe group (positive mesomeric effect) was part of the N-aryl functionality and the  $\pi$ -acceptor CN group (negative mesomeric effect). However, the substituted aromatic imines with same  $\pi$ -donor/acceptor groups did not exhibit significant red shift in  $\pi\pi^*$  absorption relative to each other (**3l** and **3m**). The computed oscillator strength of  $\pi\pi^*$  band is significantly increased in substituted imines (**3j-m**) compared to unsubstituted imine **3a**.<sup>20</sup>

Similar to alkenes, *E-Z* isomerization is also one of the major deactivation pathways for photoexcited imines (*cf.* Section 3). The presence of more than one *E* and *Z* form is also feasible

owing to the conformational flexibility of imines depending upon the structure. In such cases, assigning the most appropriate *E* or *Z* form to the experimentally observed UV spectra can become a challenging task. To address this issue of conformational complexity in imines, Amati and co-workers<sup>21</sup> utilized computational simulation of UV spectra and comparing them to the observed spectral transitions in imine. They utilized this approach to assign the spectral transitions in heteroaromatic imine **3n** that featured different conformations (conformers A-D; Figure 3) in the *trans*-isomers. By utilizing the experimental absorption spectrum in conjunction with computational results the individual conformer transition was assigned in **3n** (conformers A-D; Figure 3).<sup>21</sup> Experimental UV-Vis spectra of **3n** in petroleum ether featured an intense absorption at 354 nm. The computed spectra for different conformations of **3n** indicated that the most intense absorptions were at 361 nm and 357 nm for conformation A and B respectively. No other conformations of comparable intensities were predicted. Thus, it was in good agreement with experimentally observed spectrum.

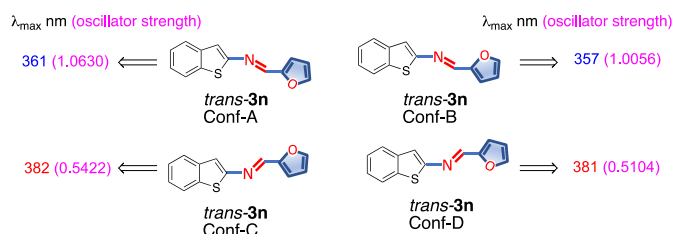


Figure 3. Influence of conformation on the UV-Vis absorption spectra of heteroaromatic imine **3n**.<sup>21</sup>

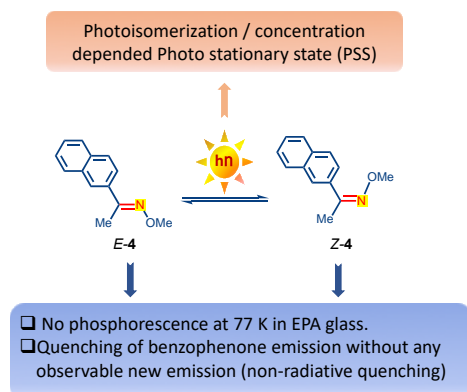
Most often, simple imines are unstable and are readily hydrolysed limiting studies related to investigation of their excited state reactivity and spectroscopic properties.<sup>10</sup> The derivatives of imines such as oximes<sup>22</sup> and hydrazones<sup>23</sup> are often stable and can act as model systems for elucidating photochemical properties of imines. The UV-Vis characteristics of these systems often reflect characteristics of simple imines.

## 2.2 Non-radiative deactivation

The non-radiative decay of excited imines plays a crucial role in determining its photochemical reactivity. As detailed in section 1.1 imines typically feature both an  $\pi\pi^*$  transition at shorter wavelengths and an  $n\pi^*$  transition at longer wavelengths. The influence of these two excited state configurations in imines can be understood based on their similarities to carbonyl  $n\pi^*$  and  $\pi\pi^*$  excited states that has been extensively studied for various conventional photochemical transformations.<sup>4,6</sup> Exciting imines to its singlet state oftentimes results in intersystem crossing to the triplet manifold. As a result, the C-N bond undergoes facile bond rotations and deactivates to the ground state (similar to excited alkenes).<sup>8,24</sup> Thus the excited state deactivation of imines (in particular acyclic imines) through photoisomerization is rather an inherent process dictated by facile bond rotation along the C-N axis.<sup>8</sup> Ooi and co-workers stated<sup>8</sup> an important distinction between the excited state of imines and the carbonyl group, where they highlighted the inherent difference in hybridization

between the hetero atoms. Excitation of carbonyl functionality transforms oxygen from  $sp$ -hybridization to oxygen atom featuring electrons in the  $2p$ -orbital that dictates its reactivity (both photophysical and photochemical process). On the other hand, imines feature a  $sp^2$ -hybridized nitrogen atom with different electronic characteristics. As photoisomerization of imines is a crucial process that dictates its reactivity, we will be discussing the intricacies of photoisomerization in section 3, while this section will mainly focus on radiative and non-radiative features of the imine chromophore.

In 1974 Padwa and Albrecht investigated the concentration dependent fluorescence of oxime ether **4** (Scheme 1).<sup>25</sup> They observed that oxime ether **4** underwent facile isomerization (*cf.* Section 3.1) from the singlet excited state. The fluorescence quenching by 1,3-hexadiene was depended on the isomer geometry. Higher quenching rate constant was observed for *E*-**4** than *Z*-**4** indicating that the *E*-isomer is more sensitive to chemical quenching than the corresponding *Z*-isomer. They also demonstrated that there was no observable phosphorescence in **4** at 77 K in EPA (5:5:2 mixture of diethyl ether, isopentane and ethyl alcohol) glass. This was rationalized due to the low intersystem crossing efficiency of the triplet state of **4** undergoing a faster non-radiative decay than the radiative transition. They substantiated this by employing benzophenone as triplet sensitizer and observed that the emission of benzophenone was completely quenched with no observable new emission from the oximes. This pointed to the non-radiative decay from the triplet state of **4** proceeding faster than the radiative decay.



**Scheme 1.** Photochemical and photophysical features in naphthyl substituted oxime ether **4**.

Mukherjee and co-workers studied the decay of the excited state of 7-ethylsalicylidenebenzylamine **5** in various solvents (Scheme 2).<sup>26</sup> They found that the non-radiative decay constants dominated over the radiative decay constants ( $k_{nr}$  and  $k_{nr}'$ ). The values varied from  $2.5 \times 10^{-8} \text{ s}^{-1}$  in methanol to  $11.9 \times 10^{-8} \text{ s}^{-1}$  in glycerol. They suggested that the out of plane bending, or torsional motion of **5** being responsible for the higher non-radiative decay rates.

Channelling the radiative decay in imines to non-radiative pathways on complexation with metal ions is employed for metal ion sensing using luminescence “turn off” strategy. For example, Mehta and co-workers<sup>27</sup> reported the turn-off

fluorescence in azaindole based bis-imine **6** for selective sensing of  $\text{Fe}^{3+}$  ion. In the absence of  $\text{Fe}^{3+}$ , they observed an intense fluorescence centered around 415 nm that was quenched upon  $\text{Fe}^{3+}$  complexation. They rationalized that the significant reduction of the fluorescence signal of the imine is due to the decrease in the non-radiative decay rates of the metal-ion bound bis-imine **6**.<sup>27</sup> They summarised that the suppression of the radiative transition was in part due to partly filled  $d$ -orbital of  $\text{Fe}^{3+}$  readily accepting the electron from bis-imine **6** upon chelation.

Solvent	$f_f$	$\tau_1$ (ns)	$\tau_2$ (ns)	$k_f$ ( $\text{s}^{-1}$ )	$k_f'$ ( $\text{s}^{-1}$ )	$k_{nr}$ ( $\text{s}^{-1}$ )	$k_{nr}'$ ( $\text{s}^{-1}$ )
Water	0.03	1.3(78)	4.9(22)	$7.7 \times 10^{-8}$	$2.0 \times 10^{-8}$	$7.5 \times 10^{-8}$	$1.9 \times 10^{-8}$
Methanol	0.05	3.8(70)	0.7(30)	$2.6 \times 10^{-8}$	$14.3 \times 10^{-8}$	$2.5 \times 10^{-8}$	$13.6 \times 10^{-8}$
Ethanol	0.02	4.1(70)	0.6(30)	$2.4 \times 10^{-8}$	$16.7 \times 10^{-8}$	$16.6 \times 10^{-8}$	$16.4 \times 10^{-8}$
Glycerol	0.27	4.5(68)	0.8(32)	$2.2 \times 10^{-8}$	$12.5 \times 10^{-8}$	$11.9 \times 10^{-8}$	$9.1 \times 10^{-8}$
Ethylene glycol	0.23	4.0(62)	1.0(38)	$2.5 \times 10^{-8}$	$10.0 \times 10^{-8}$	$9.4 \times 10^{-8}$	$7.7 \times 10^{-8}$

Excited state reactions of cyclic imines gained attention as the ring would enhance the excited state reactivity by preventing the non-radiative decay to the ground state via twisting/ photoisomerization along the C-N axis. Tokumaru and co-workers<sup>28</sup> found that the cyclic amines **7a-d** had triplet lifetimes ranging from 0.1 s to 0.8 s (Figure 4) featuring a  $\pi\pi^*$  excited-state. They also observed an increase in the triplet lifetimes when the substituents were changed from alkyl (ethyl, benzyl) functionality to aromatic functionality (phenyl). The lifetime varies as 0.8 s in **7a** with higher conjugation compared to 0.12 s in **7b** with less conjugation. This indicated that the increased conjugation contributed to the emissive  $\pi\pi^*$  state. This was also supported by solvent studies (Figure 4) where triplet lifetimes at 77 K were increased by stabilization in polar solvents (eg. EPA glass), compared to nonpolar solvents (methylcyclohexane glass).<sup>28</sup>

Solvent		<b>7a</b>	<b>7b</b>	<b>7c</b>	<b>7d</b>
EPA	$\lambda_{max}$ (nm)	465, 495	525, 510	540	530
	$E_T$ (kcal/mol)	61.5, 57.8	54.5, 56.1	53	54.0
	$\tau_T$ (s)	0.8	0.12	0.3	0.6
MCH	$\lambda_{max}$ (nm)	495	520	510	500
	$E_T$ (kcal/mol)	57.8	55.0	56.1	57.2
	$\tau_T$ (s)	0.2	0.08	0.18	0.6

**Figure 4.** Maximum wavelength ( $\lambda_{max}$ ), corresponding triplet energy ( $E_T$ ) and lifetimes of cyclic imines **7a-d** at 77K in EPA (5:5:2 mixture of diethyl ether, isopentane and ethyl alcohol) and methylcyclohexane (MCH).

### 2.3 Radiative deactivation of imines

Imines also display a rich photophysical features in which they decay to the ground state through a radiative pathway. This has been explored extensively by employing imine derivatives and their metal complexes as turn-on sensors.<sup>29</sup> For the scope of this review we will only highlight the radiative feature of simple imines. Readers are encouraged to other literature reviews on topics related to the use of imines as sensors in organic and inorganic systems.<sup>30</sup>

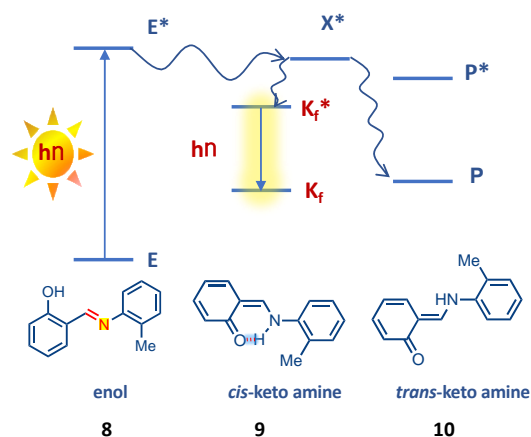


**Figure 5.** Photophysics of the *cis* and *trans*-keto form of *N*-salicylideneanilines (**8**) on photoexcitation giving rise to a photochromic state followed by formation of *cis* and *trans* keto-amine.

The rich photophysical features of imines are explored extensively for its photochromic features (*cf.* Section 3.2). One of the earliest studies related to the photophysical features of imines was performed by Nakamura and co-workers.<sup>31</sup> They examined the excited state kinetic features of *N*-salicylideneanilines **8** (Figure 5). Photoexcitation of salicylideneanilines **8** (enol-form) resulted in the formation of a photochromic *cis*-keto-amine **9** and *trans*-keto-amine **10**. Interestingly only the *cis*-keto-amine **9** showed fluorescence with two distinct lifetimes *viz.*, long lived and short-lived components. The long-lived component was attributed to the photochromic species, and the short-lived component was attributed to the excited precursor on the higher vibrational excited state. The decay time of the photochromic species in viscous solvent (liquid paraffin) was longer compared to less viscous solvents (mixture of isopentane and methyl cyclohexane). This suggested the involvement of hydrogen transfer in the photochromic state accompanied by a geometric change that was sensitive to the viscosity of the solvent. Their picosecond kinetic analysis revealed the existence of an excited intermediate prior to the formation of the photochromic *cis*-keto-amine **9** excited state (Figure 5). Thus the study gave insights about the photochromic aspects of imines (*cf.* Section 3.2).

Sliwa and co-workers<sup>32</sup> detailed the photophysical features of 2-hydroxybenzylideneaniline **11** using femtosecond spectroscopy. They were able to uncover the photodynamic features in imine **11** that displayed two competing processes both in the gas phase and in acetonitrile namely – a) the

rotational isomerism leading to twisted enol **12** and b) excited state intramolecular proton transfer (ESIPT) leading to keto-amines **13** and **14** (Figure 6).<sup>32</sup> Their spectroscopic analysis revealed that the proton transfer and rotation occurred in within 100 fs in the gas phase that was confirmed by simulations.<sup>33</sup> By employing nanosecond transient absorption (355 nm), the first excited state of **11** resulted in ESIPT photo-products with a quantum yield of 12%. Excitation of **11** to the higher excited state (266 nm) led to **12** as the major product with a quantum yield of 23%.

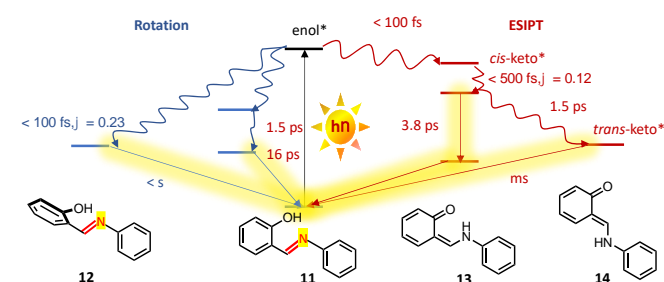


**Figure 6.** Photo physics of 2-hydroxybenzylideneaniline, rotation of the molecule gives the twisted enol and ESIPT results in *cis* and *trans*-keto forms (**13**, **14**).

Ernsting and co-workers proposed an adiabatic model for ESIPT in 2,2'-hydroxybenzoxazole **15** (Figure 7)<sup>34</sup> where they observed a major structural reorganisation and large Stokes shift around 6000 cm<sup>-1</sup>. Femtosecond pump probe experiments of **15** in cyclohexane at 298 K revealed a broad transient absorption that decayed with a time constant of 60 fs (Figure 7). The mobile hydrogen distance for the excited state intramolecular proton transfer was calculated to be around 0.41 Å.

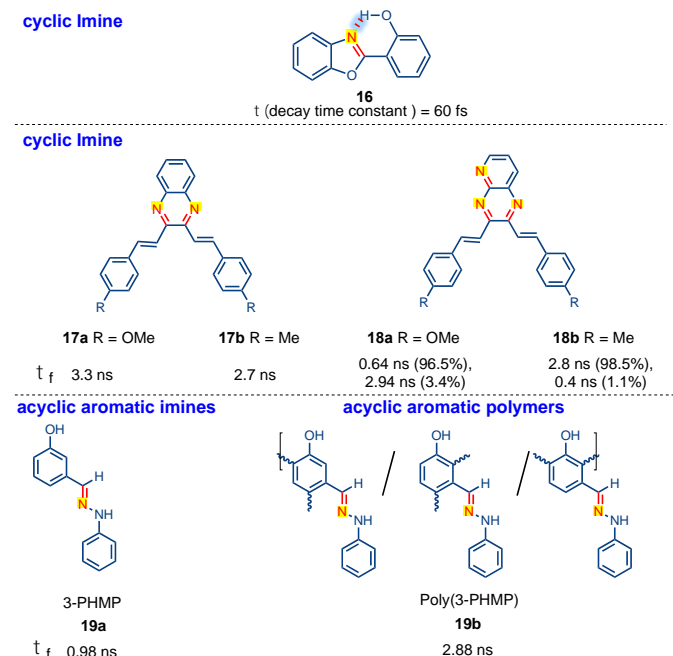
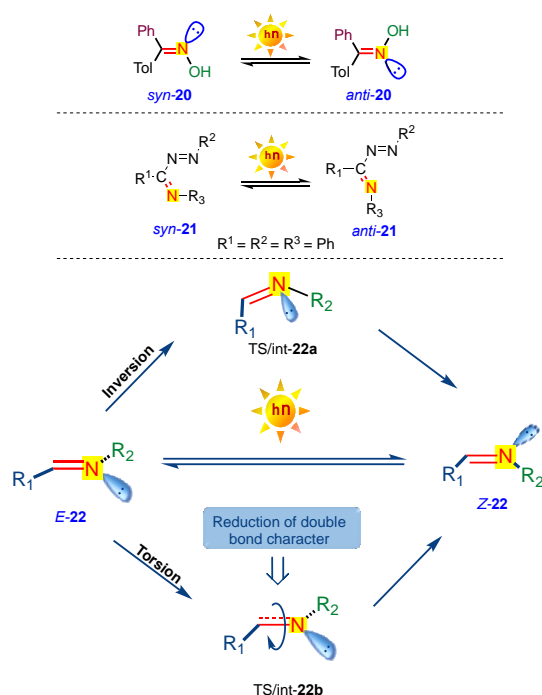


**Figure 7.** Top: Adiabatic model for ESIPT in 2,2'-hydroxybenzoxazole **15**. Middle: Fluorescence lifetimes of quinoxaline derivatives (**16** and **17**). Bottom: Fluorescence lifetimes of 3-((2-phenylhydrazono)methyl)phenol (3-PHMP, **18**) and Poly(3-PHMP, **19**) in DMF.

Perumal and co-workers reported the lifetimes of various quinoxaline derivatives **16** and **17** (Figure 7).<sup>35</sup> These derivatives had lifetimes in the nanosecond range and could be tuned with various substitutions. Introducing electron donating groups resulted in an increase in lifetime of **16a** (~3.3 ns) compared to methyl substituted derivative **16b** (~2.7 ns). For common imines the *cis-trans* isomerization (*cf.* Section 3.1) was very fast and was detected only at low temperatures.

Altering the excited state lifetimes of imines by incorporating them within a dendrimer backbone was explored by Demir and co-workers (Figure 7).<sup>36</sup> They utilized 3-PHMP **18** as the model system that showed a fluorescence time of 0.98 ns in DMF. By functionalizing them as part of a polymer backbone **19** the fluorescence lifetime increased to 2.88 ns.<sup>36</sup> The enhancement of fluorescence lifetime was attributed to the increased conjugation in the polymer **19**.



**Scheme 3.** Photoisomerization of imines **20** (top) and **21** (middle). Inversion and torsion pathways for photoisomerization of imines (bottom).

3-bottom) either via linear inversion or rotation around C-N axis (torsion). To attain this geometrical change between isomers, torsion mechanism involves twist across the C-N double bond that results in the reduction of the double bond character of the imines in the transition state when compared to the ground state (Scheme 3-bottom). In contrast to this, inversion mechanism there is increase in the N=C-R bond angle in the transition state. The nature of the substituent often determines the isomerization pathway. For example, electron donating aryl substituents on nitrogen preferred the torsion mechanism, while electron withdrawing aryl substituent favored the inversion mechanism.<sup>5</sup>

**Table 1:** Photoisomerization of various imines reported in the literature.<sup>20,40-42</sup>

Entry	<i>syn</i>	<i>anti</i>	References
1			40
PSS: <b>Z-23a</b> : <b>E-23a</b> = 2.2:1 Pentane, $h\nu \sim 250 \text{ nm}$			
2			41
PSS: <b>Z-23b</b> -64% at 0.003 M <b>Z-23b</b> -42% at 1.35 M Pentane, $h\nu \sim 313 \text{ nm}$			
3			20
c: X, Y = CH <sub>3</sub> d: X, Y = CN e: X = OCH <sub>3</sub> , Y = CN f: X = CN, Y = OCH <sub>3</sub> g: X = CN, Y = CH <sub>3</sub> h: X = OCH <sub>3</sub> , Y = CH <sub>3</sub>			
4			42

### 3. Photochemical reactivity of imines

#### 3.1 Photoisomerization

In 1890, Hantzsch<sup>37</sup> and co-workers reported that the oximes **20** undergo geometric isomerization in the presence of UV light (Scheme 3-top). One of the earliest report on photo-induced isomerization of C=N bond was reported by Kuhn and Weitz (Scheme 3-middle).<sup>38</sup> The spectroscopic details of *cis-trans* photoisomerization of imines was investigated by Fischer and Frei.<sup>39</sup> In general, the *E*-isomer of 1,2-substitued imines is more stable than the corresponding *Z*-isomer similar to what is typically expected for 1,2-substitued olefins.<sup>38</sup> However, compared to olefins, the thermal barrier for *Z*-to-*E* conversion is low in imines and hence they typically equilibrate at ambient conditions. Imines undergoes *E/Z* photoisomerization (Scheme

Although there are several reports published,<sup>40,42-44</sup> the mechanism of the C=N photoisomerization in imines is obscured due to the complexity and dynamics prevalent in the excited state(s). This is in addition to the low thermal barrier for ground state isomerization. The *E-Z* photoisomerization of imines is also referred to as *syn-anti* isomerization in literature.<sup>45</sup> To adhere to IUPAC conventions, we will use the *E/Z* nomenclature instead of *syn-anti* nomenclature that is employed for detailing the photoisomerization of imines in literature.<sup>45</sup>

Undoubtedly photoisomerization of C-N double bond is a major deactivating pathway for the radiationless decay of the excited imine functionality. This often manifests in determining the photoreactivity of imines.<sup>4</sup> Photoisomerization of imines from both singlet and triplet states have been reported.<sup>46</sup> To

highlight the importance of photoisomerization, we have selected few of the relevant examples involving aromatic imines (Table 1).<sup>20,40–42</sup>

The original report on the photoisomerization of oximes **20** was reported by Hantzsch and co-workers in 1890,<sup>37</sup> was explained mechanistically by Padwa and Albrecht.<sup>40,41</sup> They employed acetophenone oxime ethers,<sup>40</sup> naphthyl substituted oxime ethers,<sup>41</sup> and ketoximes<sup>40</sup> as model systems to elucidate the mechanistic intricacies of photoisomerization (Table 1). The alkoxy group on the imine nitrogen increased the thermal energy barrier for isomerization that manifested in the lower rate for of thermal interconversion between the *Z*- and *E*-C=N isomers. This increased thermal barrier provided a suitable platform to investigate the photoisomerization in imines by side-stepping the thermal process.<sup>40</sup> Irradiation of oxime **23a** (concentration range 0.01–0.3 M) at ~253 nm gave a *Z*-*E* ratio of 2.2:1. The quantum yield for *Z*-**23a** → *E*-**23a** was 0.29 and *E*-**23a** → *Z*-**23a** interconversion was 0.37.<sup>25</sup> The photostationary state (PSS) for the isomerization process upon direct irradiation was calculated using equation 1 and was found to be 0.4 (@ 253 nm in pentane).<sup>40</sup> Detailed spectroscopic investigation were carried out on oxime ethers **23a–b** that revealed that the photo-equilibration happened through an excited singlet state.<sup>40,41</sup> This isomerization can also be induced by triplet excitation by using various triplet sensitizers with different triplet energies.<sup>41</sup>

$$\frac{[Z]}{[E]} = \frac{\epsilon_E \Phi_{[E \rightarrow Z]}}{\epsilon_Z \Phi_{[Z \rightarrow E]}} \quad \text{Eq. 1}$$

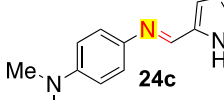
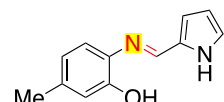
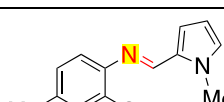
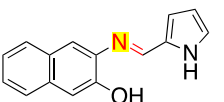
**Equation 1:** Extinction coefficient  $\epsilon$  and  $\Phi$  denotes quantum yield for *E* and *Z* configuration.

Padwa and co-workers also disclosed that the concentration of the imine played a crucial role in the photoisomerization process. Photoisomerization of *anti*-*N*-(*O*-methyl)-2-acetonaphthone oxime *anti*-**23b**<sup>41</sup> at 313 nm resulted in the *Z*-**23b**. The photostationary state was 64% favouring the *Z*-isomer when a concentration of 0.003 M **23b** was employed for photoisomerization while, it decreased to 42% *Z*-**23b** at a concentration of 1.35 M (Table 1; entry 2). Based on this observation, it was rationalized that high concentration favoured the more stable *E*-isomer. Contrary to the excited singlet state isomerization, the triplet state isomerization quantum yield of oxime ethers (e.g. **23a**) were independent on the *E*-isomer concentration and only marginally dependent on the *Z*-isomer concentration. It was also revealed that the photoisomerization of oximes (e.g. **23b**) was dependent on the temperature and the solvent. At higher temperatures the contribution of the *E*-isomer was diminished ( $[Z\text{-}23a]/[E\text{-}23a]$  ratio in pentane (0.1 M) was  $0.92 \pm 0.03$  at 25 °C and upon increasing to 80 °C the ratio increased to  $1.20 \pm 0.05$ . Similarly, the  $[Z\text{-}23a]/[E\text{-}23a]$  ratio in pentane at 0.003 M was  $1.80 \pm 0.06$  at 25 °C and increasing the concentration to 0.05 M the ratio decreased to  $1.11 \pm 0.05$ . Changing the solvent to benzene (1.35 M), the  $[Z\text{-}23a]/[E\text{-}23a]$  ratio was  $0.72 \pm 0.04$  at 25°C. Based on this observation it was postulated that the imines likely formed excited state aggregates (excimers) that is responsible for the

observed concentration, temperature and solvent dependence of photoisomerization.<sup>25</sup>

Raposo and co-workers investigated the kinetics of *cis*-to-*trans* thermal re-isomerization of various pyrrolidine imines **24a–g** (Table 2).<sup>42</sup> They found that on changing the substitution at the *para*-position of the aniline increased the half lifetime of the *cis*-imine at room temperature. This led to lower rates for *cis*-*trans* re-isomerization leading to an appreciable change in the UV-Vis spectral characteristics (*cf.* Section 3.2, photochromism).

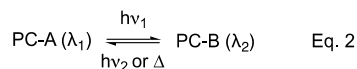
**Table 2:** Kinetics of thermal isomerization of imines **24a–g**.<sup>42</sup>

Entry	Imines	Photostationary state reaction parameters	
		% <i>cis</i>	$k_A$ (s <sup>-1</sup> )
1		>6	0.051
2		>24	0.019
3		>40	0.015
4		>8	0.093
5		>12	0.070
6		>5	0.200
7		>3	0.022

### 3.2 Photochromism

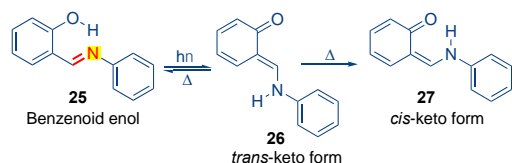
Photochromism is the phenomenon exhibited by the compounds that undergo reversible change of colour upon irradiation of light of a specific wavelength typically in the UV and/or visible region. The reversible change can either be induced by heat or light. The typical characteristics of photochromic compounds are given below a) The photochromic compounds e.g. PC-A and PC-B (Eq. 2) should have different absorption profile i.e., absorption maxima of  $\lambda_1$

for PC-A and  $\lambda_2$  for PC-B; b) The two compounds should possess optimal stability at the irradiation wavelength; and c) The compounds should display reversible behaviour when subjected to external stimuli (eg. light, heat etc.) and should be stable to those stimuli.<sup>47</sup> While there are different classes of photochromic compounds, this review highlights photochromism based on imines. Readers are encouraged to refer other reviews related to photochromism based on other class of compounds.<sup>48</sup>



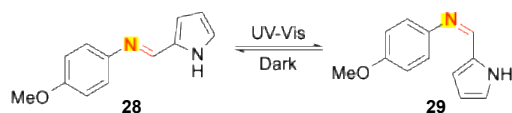
**Equation 2:** PC- photochromic state of A, B and  $\lambda_1, \lambda_2$  are specific wavelengths.

One of the first reports on photochromism in imines was reported by Becker and co-workers.<sup>49</sup> They reported the photochromic behaviour of salicylideneaniline-enol **25** (Scheme 4) which upon UV irradiation underwent photo-enol tautomerism to the corresponding *trans*-keto-anil-**26**. The *trans*-keto-anil-**26** thermally isomerized to the *cis*-keto-isomer **27**. The photo-tautomerization involved a hydrogen transfer from the phenolic oxygen to the excited imine. The reaction featured a color transition from yellow colored enol **25** to red colored *trans*-keto-**26** (absorption maxima at  $\sim 480$  nm).<sup>49</sup>



**Scheme 4.** Photochromism in imine **25**.

Ottolenghi and co-workers<sup>44</sup> explained the plausible pathway and also the primary steps that are associated with photochromism in anils i.e., imines derived from ortho-hydroxyaromatic aldehydes. They investigated the mechanistic aspects of photochromism in **25** that was dependent on the reaction media. Flash photolysis studies in fluid solution showed both intramolecularly H-bonded enol-form-**25** and *cis*-keto-**27** form yield the *trans*-keto isomer **26** as a common photoproduct. Upon changing the media to a rigid paraffin glass they observed photoisomerization of enol to the *trans*-keto-isomer and not the conversion of *cis*-keto form to the corresponding *trans*-keto-isomer.<sup>44</sup>



**Scheme 5:** Photochromic equilibrium of pyrrolidene imine **28**.

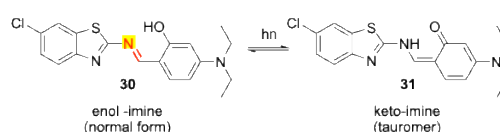
Photochromism in imines has been widely reported with benzylidene aniline type imines and Schiff bases though other type of imines were also well known.<sup>20,42,47,49</sup> Raposo and co-workers<sup>42</sup> reported the photochromic equilibrium of *trans*-pyrrolidene imine **28** (Scheme 5) that underwent photoisomerization upon UV-Vis irradiation to the corresponding *cis*-isomer **29**. The *cis*-isomer **29** underwent

thermal isomerization (in dark) to the more stable *trans*-form **28**. They also performed solvent effect on photochromism and concluded that solvents played a minimal role in determining the photochromic behaviour of pyrrolidene type imines.<sup>42</sup>

### 3.3 Excited state intramolecular proton transfer reaction of imines

Excited state intramolecular proton transfer reaction (ESIPT) usually occurs when proton transfers from a one atom to another atom within the same molecular framework upon irradiation. ESIPT reactions are very useful processes in modulating chemical pathways possessing multiple industrial applications. Usually ESIPT reactions could be accompanied by excited state intramolecular charge transfer reactions (ESICT) as well, if the electron donor and acceptors are present in the same skeleton. Hence both ESIPT/ESICT processes could occur in the same system and can be often decoupled by introducing suitable substituents in the parent molecule. These photoinduced ESIPT reactions are highly sensitive towards the microenvironment such as polarity of the solvent, substituents, temperature, pH of the medium etc. As detailed in Scheme 4, photochromism of anils could in general be classified as an ESIPT process if the proton transfer from the enol to keto form (or vice versa) occurs in the excited state. We will limit our discussions related to ESIPT reactions of imines (Schiff bases) because of its rich photochemical and photophysical properties considering its various applications in this section.<sup>50</sup> We have detailed the ESIPT mediated cycloaddition reactions of imines in section 3.11.

Ghosh and co-workers<sup>50</sup> investigated ESIPT reactions of heterocyclic Schiff base **30** in various solvents (Scheme 6). In non-polar heptane, they observed dual emission from both the excited enol-imine (**30\***) and the excited state of the tautomer keto-amine (**31\***) species. Upon increasing the solvent polarity, they observed a decrease in ESIPT transition emission band. The ESIPT emission was not observed in polar methanol. They postulated that increasing polarity of solvent molecule, enhanced the intramolecular charge transfer in excited enol-imine (**30\***) (ESICT) that essentially diminished the ESIPT process.

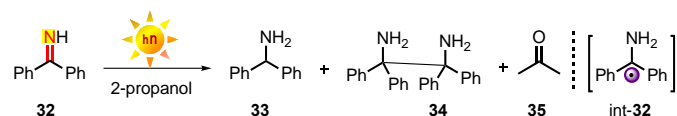


**Scheme 6.** Keto-enol tautomerization of imine **30**.

### 3.4 Photoreduction

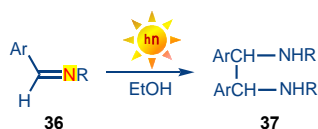
Photoreduction involves the use of light to alter the oxidation state of chromophores typically by adding hydrogen(s) from an abstractable source (e.g. solvents).<sup>6</sup> One of the earliest reports on photoreduction involving imines was disclosed by Short and co-workers.<sup>51</sup> They reported the irradiation (Scheme 7) of benzophenone ketimine **32** in isopropanol leading to the formation of reduced amine **33**, reduced coupling product **34** (pinacol amine product) and ketone **35** (from the solvent). The reaction was postulated to occur from the  $n\pi^*$  excited state of **32** in a process that

analogous to the photoreduction of benzophenone in the presence of isopropanol.<sup>8</sup> The photoreduction quantum efficiency was found to be 0.03 relative to the photoreduction of benzophenone in 2-propanol. In addition, the rate of photoreduction was retarded in the presence of naphthalene that served as a triplet quencher indicating that the reaction likely involved a triplet species.



Scheme 7. Photoreduction of benzophenone imine **32**.

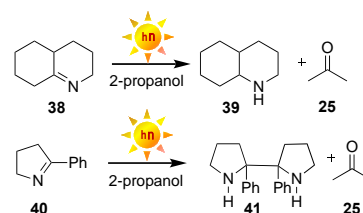
Similar to the reaction of ketimine **32**, Usherwood and co-workers<sup>52</sup> investigated the photoreduction and dimerization of benzaldehyde aldimines **36** leading to the formation of the pinacol type product **37** (Scheme 8). The initial mechanism proposed by Short and co-worker<sup>51</sup> that involved the excitation of imine was reinvestigated by Padwa and co-workers (Scheme 8).<sup>53</sup> They suggested that the reaction while analogous to the photoreduction of aryl ketones,<sup>6</sup> doesn't involve excited state of imine. Their proposed mechanism was based on the following observations - a) although photoreduction of imine **36** was efficient in ethanol, it was not efficient in 2-propanol, a well-known solvent for photoreduction of benzophenone; b) unlike aryl ketone photoreduction, the substituents on the aryl system did not affect the efficiency of the photoreduction of imines; c) photo-excitation of **36** at 254 nm (where the imine predominantly absorbed) did not result in the photoreduction product, while photoreduction was observed when the irradiation was switched to 313 nm.; and d) photoreduction quantum yield was 0.58 in the presence of benzophenone as a sensitizer (in spite of the benzophenone phosphorescence not being quenched by imine). Based on these observations, Padwa and co-workers attributed the photoreduction of imines to partial hydrolysis in the aqueous media leading to benzaldehyde (for benzaldehyde aldimines). The carbonyl species competed favorably with imine as a light absorbing species at longer wavelengths (>310 nm) and acted as a sensitizer. This was consistent with the observed photoreduction of *N*-alkylimine in 2-propanol in the presence of low concentrations of triplet photosensitizers such as benzaldehyde and benzophenone.



Scheme 8. Dimerization of benzaldehyde imine **36**.

Hornback and co-workers<sup>54</sup> reported the photoreduction of cyclic imines **38** and **40** which upon irradiation underwent reduction (Scheme 9) in 2-propanol to give **39** (yield 98%) and **41** (yield 87%) as the major product respectively. Their study involved the incorporation of the carbon-nitrogen double bond into a ring system was geared towards investigating the involvement of the twisting/isomerization around the C-N bond during the photoreduction. By incorporating the imine

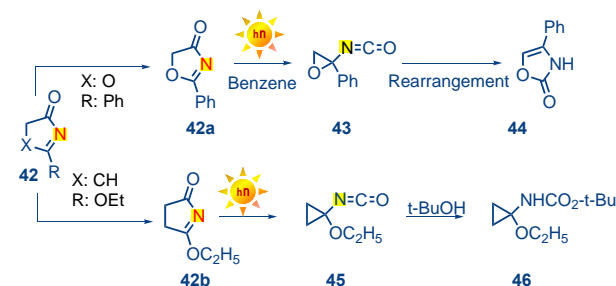
functionality as part of a cyclic system prevented photo isomerization as deactivation mechanism.



Scheme 9. Photoreduction of cyclic imines **38** and **40**.

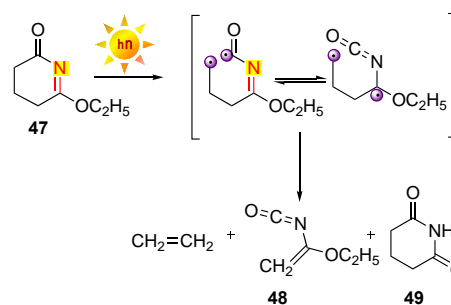
### 3.5 Photofragmentation

Koch and co-workers<sup>55</sup> reported the photofragmentation of cyclic keto imino ethers **42a-b** (Scheme 10). 2-Phenyl-2-oxazoline-4-one **42a** underwent  $\alpha$ -cleavage / photofragmentation upon irradiation in benzene solution resulting in the isocyanate **43**. The isocyanate underwent a rearrangement to form the oxazolidinone product **44**. Similarly, the ethoxy-derivative **42b** underwent  $\alpha$ -cleavage/ photofragmentation to form the corresponding isocyanate **45** that was subsequently trapped by alcohol to form carbamate **46**. The reaction of **42b** was rationalized to occur through an  $n\pi^*$  singlet excited state localized on the imine chromophore.<sup>55</sup>



Scheme 10. Photofragmentation of cyclic imine derivatives **42a** and **42b**.

In order to explain the mechanism of photofragmentation Koch and co-workers<sup>55</sup> examined the photolysis of homologous 6-ethoxy-4,5-dihydro-2-pyridone **47** that gave ethoxyvinyl isocyanate **48** as the major product and imide **49** as the minor product along with extrusion of ethylene (Scheme 11). Their investigation revealed that the fragmentations proceeded through an  $n\pi^*$  excited state via a Norrish type I mechanism. Based on quenching studies, they proposed the reaction likely involves a singlet excited-state or a short lived triplet excited state.<sup>55</sup>

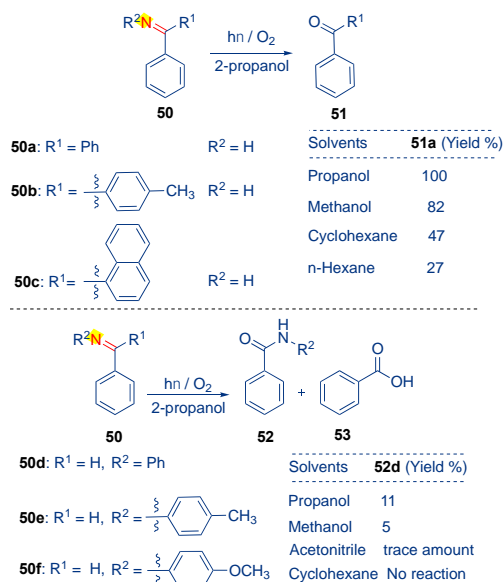


Scheme 11. Photolysis of 6-ethoxy-4,5-dihydro-2-pyridone **47**.

### 3.6 Photooxidation

Toshima and Hirai reported the photooxidation of ketimines **50a-c** and aldimines **50d-f** (Scheme 12). Irradiation of ketimine **50a** in 2-propanol in the presence of O<sub>2</sub> led to the formation of the benzophenone **51a** (Scheme 12-top).<sup>56</sup> The photooxidation efficiency was dependent on the solvent with quantitative yields of the product 2-propanol, whilst 82% yield was observed in methanol. In non-polar solvents like cyclohexane and hexanes, the yields were 47% and 27% respectively. The solvent dependence was rationalized based on the hydrogen donating capability.<sup>56</sup> Similar reactivity was observed for *para*-tolyl-substituted ketimine **50b**. On the other hand, naphthalene substituted ketimine **50c** did not undergo photooxidation.

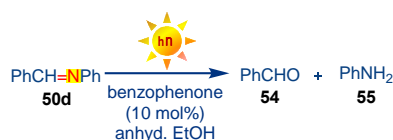
Unlike ketimine **50a-c**, aldimines were found to exhibit differential reactivity (Scheme 12-bottom).<sup>56</sup> Photooxidation of aldimines **50d-f** led to the corresponding benzamides **52d-f** in less than 10% yield along with benzoic acid **53** (15% yield) along with the recovery of the unreacted aldimines (50-63%).



Scheme 12. Photooxidation of 1,1-diphenylmethyleimine **50a-f**.

### 3.7 Light induced hydrolysis

Kan and Furey<sup>57</sup> reported a benzophenone sensitized photolysis of aldimine **50d** in anhydrous ethanol leading to benzaldehyde **54** (74% yield) and aniline **55** (80% yield). Hydrolysis of **50d** was also observed under dark conditions albeit in low yields (12% yield of **54** and 13% yield of **55**).<sup>57</sup>

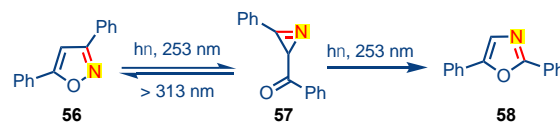


Scheme 13. Schematic representation of photolysis of benzylidene aniline **50d**.

### 3.8 Photorearrangement

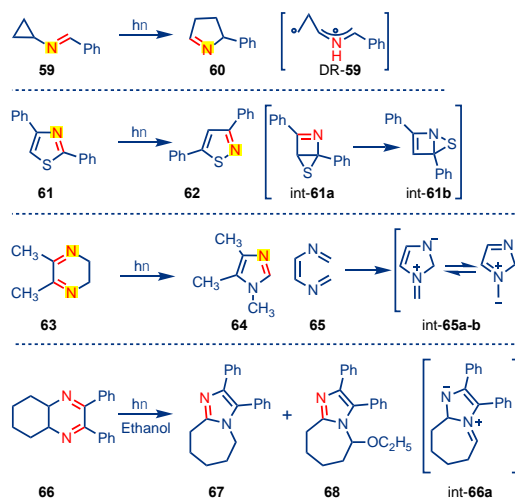
Ullman and Singh reported the photo-rearrangement of 3,5-diarylisoxazoles **56** that showed wavelength dependence.

Irradiation of diaryloxazoles **56** at ~253 nm led to oxazole **58**, while azirine **57** was formed as an intermediate which upon irradiation at >300 nm led to **56** (Scheme 14).<sup>58</sup> The wavelength dependence on product distribution was rationalized based on experimental observation in which oxazole **58** was observed in higher efficiency than azirine **57** at lower irradiation wavelengths. This led to the suggestion that oxazole **58** was likely derived from azirine **57** upon photoirradiation at 254 nm, while at 300 nm, azirine **57** rearranged back to isoxazoles **56**. Thus, this rearrangement sets an epitome for the photo rearrangement of imines.



Scheme 14. Wavelength dependent photorearrangement of **56**.

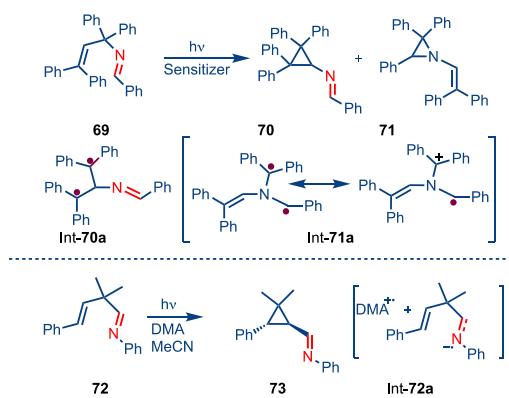
Heterocyclic system featuring C-N double bond showcases a rich diversity in undergoing photoinduced rearrangements. As shown in Scheme 15, rearrangement of acyclic and heterocyclic imines has been reported.<sup>59-61</sup> Sampedro and co-workers<sup>59</sup> reported the photorearrangement of *N*-cyclopropylimines **59** (Scheme 15-top) leading to the formation of pyrrolines **60**. The reaction was postulated to occur through non-equilibrated excited state diradical DR-**59**. Kojima and co-workers<sup>61</sup> reported the photo-rearrangement of phenylisothiazole **61** (Scheme 15-middle) leading to thiazole **62**. Although the exact mechanistic details were not deciphered, they suggested the involvement of bicyclic intermediates int-**61a-b** in the reaction pathway. Similarly, Miesel and co-workers<sup>60</sup> reported the rearrangement of six-membered 2,3-dihydro-5,6-dimethyl pyrazines **63** (Scheme 15-bottom) in ethanol leading to 1,4,5-trimethyl imidazole **64**. They proposed an initial retro-[4+2]-photolytic ring opening to form the triene **65** that subsequently rearranges to **64** via intermediate **65a-b**. Similarly, photolysis of quinoxaline **66** in aqueous ethanol proceeded through int-**66a** and resulted in isomeric azepine **67** and **68** in 9% and 62% respectively (Scheme 15-bottom).



Scheme 15. Photorearrangement of acyclic and heterocyclic imines.

### 3.9 Aza-Di- $\pi$ methane rearrangement of imines

Armesto and co-workers<sup>62,63</sup> investigated the aza-variant of the di- $\pi$ -methane rearrangement of both 1-azadienes and 2-azadienes (Scheme 16). Photoirradiation of 2-azadiene **69** in the presence of 9,10-dicyanoanthracene (DCA) resulted in the formation of aza-di- $\pi$ -methane rearrangement products **70** and **71** (Scheme 16-top). Similar reactivity was observed when acetophenone was employed as a triplet sensitizer. Changing the position of the imine nitrogen i.e., 2-azadienes (e.g. **69**) to 1-azadienes (e.g. **72**) revealed that the product distribution was depended on the location of the imine nitrogen. For example, photoinduced aza-di- $\pi$ -methane rearrangement involving 1-azadiene **72** in the presence of dimethyl amine (DMA) resulted in **73** as the major product. The reaction was postulated to occur via a photoinduced electron transfer reaction involving DMA as an electron donor and 1-azadiene **72** as an electron acceptor leading to radical cation/anion intermediates (Scheme 16-bottom).

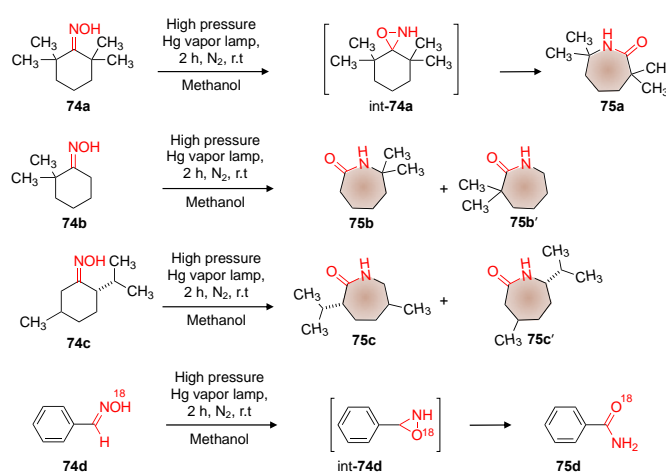


Scheme 16. Aza-di- $\pi$ -methane rearrangement of imines.

### 3.10 Ring expansion reaction involving imines

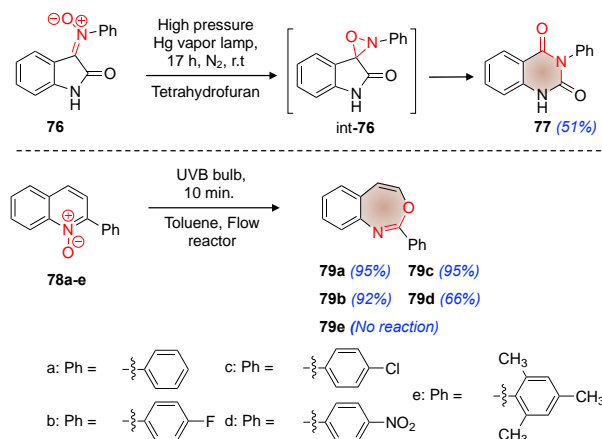
Imine scaffolds featuring an exocyclic imine double bond (e.g. *N*-oximes **74** or *N*-oxides (nitrones) **76** and **78**) are reported to undergo photochemical ring expansion (Scheme 17 and 18). The reaction involved formation of an unstable oxaziridine intermediate that ring expanded to form the final product. Just and co-workers<sup>64–66</sup> reported photochemical Beckmann rearrangement of cyclohexanone oxime derivative **74a** to caprolactam derivative **75a** (Scheme 17). Irradiation of 2,2,6,6-tetramethylcyclohexanone oxime **74a** in methanol resulted in the formation of 2,2,6,6-tetramethylcaprolactam **75a** in 60% yield (Scheme 17) and the reaction was postulated to occur through int-**74a** (Scheme 17).<sup>66</sup> This photochemical reaction addressed the issue related to Beckmann rearrangement of  $\alpha$ -substituted oximes that either did not react or gave diminished yield under thermal conditions. For  $\alpha$ -*tetra*-substituted cyclohexanone oxime which does not undergo thermal Beckmann rearrangement,<sup>66</sup> a facile rearrangement was observed under photochemical conditions. They also investigated the effect of  $\alpha$ -substitution and showed that even unsymmetrical cyclohexanone oxime (e.g. **74b**) underwent photochemical Beckmann rearrangement to form regioisomeric amides **75b** and **75b'** (Scheme 17). To understand the

mechanistic aspects, they investigated the photorearrangement of oxime **74c** that featured a chiral centre at  $\alpha$ -position. Photochemical Beckmann rearrangement of **74c**



Scheme 17. Ring expansion reaction involving oximes.

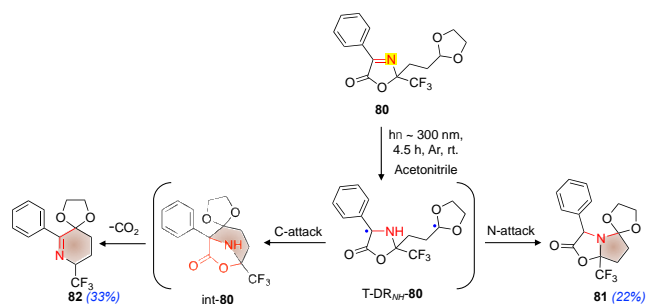
gave amides **75c** and **75c'** with retention of configuration (Scheme 17). This supported the formation of oxaziridine intermediate over radical intermediate(s). They also revealed that changing the solvent from methanol to isopropanol resulted in radical intermediates. The formation of oxaziridine intermediate during photochemical Beckmann rearrangement was further supported by the work of Tabata and co-workers.<sup>67</sup> They investigated the photorearrangement of <sup>18</sup>O labelled benzaldoxime **74d** leading to amide **75d** that featured isotope incorporation in the amide carbonyl. This suggested the formation of the oxaziridine intermediate during photoinduced Beckmann rearrangement.<sup>67</sup>



Scheme 18. Ring expansion reaction involving imine *N*-oxide. The product yields are provided in parenthesis.

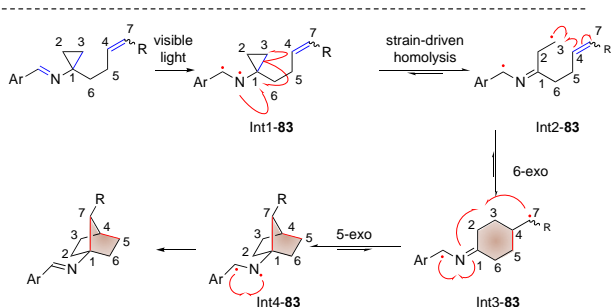
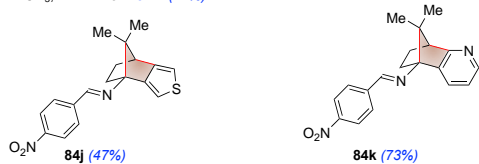
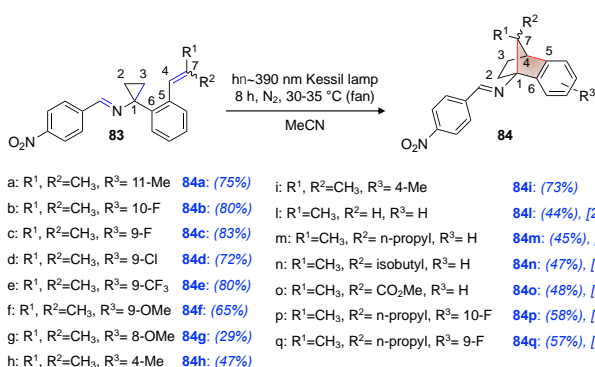
Photochemical rearrangement of imine *N*-oxides are also reported.<sup>68,69</sup> Sasaki and co-workers<sup>68</sup> reported photochemical ring enlargement of *N*-(2-oxo-3-indolylidene)-aniline-*N*-oxide **76** (Scheme 18-top). Irradiation of **76** in tetrahydrofuran resulted in the formation of 3-phenyl-2,4-(1*H*,3*H*)-quinazolinone **77** in 51% yield (Scheme 18-top) through an oxaziridine intermediate int-**76**. Similar photorearrangement of

endocyclic imines was recently reported by Smith and co-workers.<sup>69</sup> Photorearrangement of *N*-oxide derivative **78**



**Scheme 19.** Ring expansion reaction involving imine double bond through hydrogen abstraction. The product yields are provided in parenthesis.

resulted in benzoazepine **79**, a pharmaceutically important skeleton (Scheme 18-bottom).<sup>69</sup> Irradiation of 2-(4-(ethoxycarbonyl)phenyl) quinoline-1-oxide **78a-d** in toluene under UVB light irradiation in a flow reactor resulted in the formation of the corresponding ethyl-4-(benzo[d][1,3]oxazepin-2-yl)benzoate **79a-d** with excellent yield (>90%). The reaction was tolerant to electron withdrawing groups at *para*-position of the phenyl ring (Scheme 18; compare **78a** vs **78b-d**). Employing a *para*-nitro-substituent on the phenyl ring (as in **78d**) resulted in lower yields (~66%). Incorporating bulky *ortho*-substituent on the phenyl ring as in **78e** did not yield any photoproduct.



**Scheme 20.** Ring expansion reaction involving cyclopropyl imines. The product yields and diastereomeric ratios are provided in parenthesis.

Hoffmann and co-workers<sup>70</sup> reported photochemical ring expansion reaction of a cyclic imine oxazolone derivative **80** (Scheme 19). Irradiation of **80** at ~300 nm in acetonitrile resulted in cyclized product **81** and ring expansion tetrahydropyridine product **82** in 22% and 33% yield respectively. In the reaction mechanism nitrogen atom of triplet excited imine double bond intramolecularly abstracts the hydrogen atom from the acetal carbon to form triplet diradical T-DR<sub>NH</sub>-**80**. This diradical bifurcates to form either the cyclized product **81** or undergoes decarboxylation and subsequent cyclization to form the ring expansion product **82** (Scheme 19).

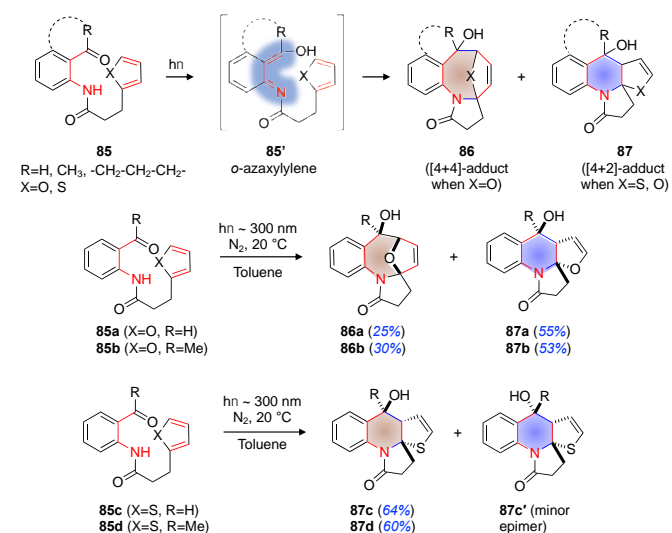
Stephenson and co-workers<sup>71</sup> reported ring expansion reaction of suitably tethered cyclopropyl imines **83** to form 1-iminonorbornanes **84** (Scheme 20-top). The reaction was quite efficient with good functional group tolerability (**83a-q**). Norbornene product with unsymmetrical substitution at the bridge head C-7, **84i-q** was formed with *anti*-selectivity. UV-Vis absorption spectra of imines **83** showed a weak absorbance around 390 nm corresponding to an n→π\* transition. Irradiation of cyclopropyl imine derivatives **83a-q** at 390 nm resulted in the formation of an electron deficient N-centred radical. This imine radical initiates the homolytic cleavage of σ bond of cyclopropyl moiety leading to int1-**83** that undergoes sequential 6-exo and 5-exo radical cyclization to form 1-iminonorbornanes with regeneration of imine double bond. Imine double bond in the final product **84** can be readily hydrolysed to generated 1-amino norbornane derivatives which are potential bioisosteres of aniline.

### 3.11 ESIPT mediated photocycloaddition involving in situ generated C-N double bond

While we had shown the involvement of ESPIT in imines during photochromism/photoisomerization (Section 3.2), this section will highlight on how to utilize the ESIPT process to generate reactive intermediate featuring C=N for synthetic manipulation. The C-N double bond generated in situ on photoexcitation can undergo photocycloaddition reaction.<sup>72-83</sup> In their pioneering work, Kutateladze and co-workers demonstrated in situ generation of C=N as a reactive functionality through excited state intramolecular proton transfer (ESIPT) of *o*-amino aromatic ketones (Scheme 21).<sup>72</sup> Photoirradiation of *o*-aminoketone **85** (Scheme 21) resulted in ESIPT to form *o*-azaxylylene **85'**. The intermediate featuring reactive C=N thus generated undergoes [4+2] and/or [4+4]-cycloaddition with suitably tethered alkenyl functionality. For example, *o*-amino aromatic ketone with furan tether **85a,b** underwent ESIPT mediated photocycloaddition leading to both [4+4]-adduct **86a,b** and [4+2]-adduct **87a,b** (Scheme 21).

However, changing the furan to a thiophene tether resulted in the exclusive formation of [4+2]-adduct **87c,d** (Scheme 21). For example, the thiophene-aldehyde **85c** underwent ESIPT mediated cycloaddition to give **87c** and its epimer **87c'**, while the thiophene-ketone **85d** gave exclusively **87d** (the epimeric product was not observed). The presence of *syn/anti* configurations with respect to the hydroxyl group and hetero atom at the bridge or annelated ring contributed to the structural diversity of the photoproducts. Irrespective of the

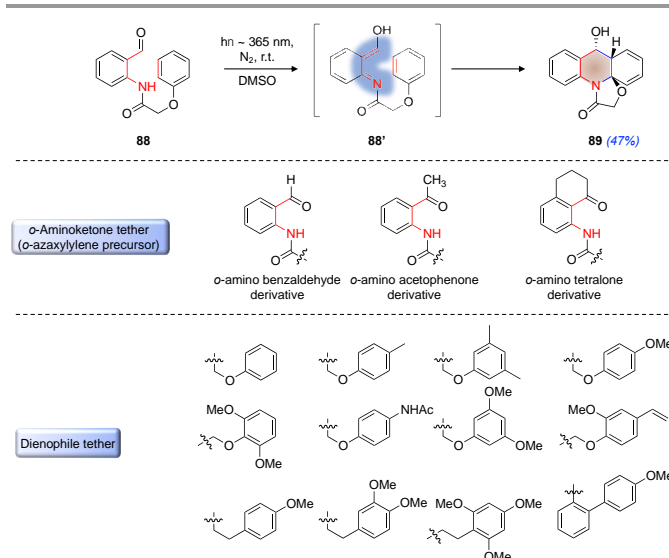
nature of the tether i.e., furan tether vs thiophene tether, *anti*-selectivity (*anti:syn* > 30:1) was observed in the [4+2]-adduct while *syn* selectivity (*syn:anti* > 30:1) was observed with [4+4]-adduct (Scheme 21). An additional aspect of this ESIPT mediated [4+2]-cycloaddition was that it featured inverse electron demand type cycloaddition, where azaxylylene acted as electron acceptor and the furan/thiophene motif acting as the electron rich dienophile.<sup>72,81</sup>



**Scheme 21.** Intramolecular photocycloaddition of *o*-azaxylylene involving C=N generated by ESIPT. The product yields are provided in parenthesis.

Photocycloaddition of *O*-azaxylylene **88** was also employed for the dearomatization of benzenoid arenes (Scheme 22-top).<sup>81</sup> Irradiation of anilide of phenoxyacetic acid **88** at ~365 nm in DMSO resulted in ESIPT leading to the formation of imine **88'** (Scheme 22-top) that subsequently underwent [4+2]-cycloaddition leading to **89** with *syn*-selectivity in 47% yield. (*syn/anti* configuration in this case refers to the orientation of benzylic hydroxyl group with respect to that of cyclohexadiene ring in the photoproduct). Reaction was quite efficient with wide substrate scope of photoprecursor with azaxylylene unit derived from *o*-amino benzaldehyde, *o*-amino acetophenone, *o*-amino tetralone, that featured amide tether derived from phenoxy acetic acid, phenyl propionic acid and biphenyl propionic acid (Scheme 22-bottom).

Kutateladze and co-workers extensively evaluated the photophysical features related to ESIPT mediated photocycloaddition of in situ generated C=N functionality to decipher the mechanism of reaction.<sup>83</sup> UV-Vis absorption spectra of **90** showed a strong absorption band that corresponded to  $\pi\pi^*$  excited state (Figure 8-top). Compounds that went ESIPT mediated photocycloaddition featured two distinct emission peaks (Figure 8-bottom).<sup>83,84</sup> The short wavelength emission band was assigned to the excited state decay of the parent compound *o*-amino aromatic ketone and the longer wavelength emission featuring a large Stokes shift was assigned to the photo-enolized tautomer.<sup>84</sup> However, *o*-azaxylylene derived from acyclic carbonyl compounds of the type **85a,b** had very weak band corresponding to ESIPT intermediate due



**Scheme 22.** Intramolecular [4+2]-photocycloaddition of *o*-azaxylylene **88** involving dearomatization of phenyl tether (top) and substrate scopes (bottom).

to non-radiative relaxation from free rotating carbonyl groups.<sup>83</sup> *o*-Azaxylylene derived from cyclic ketone **85e** (tetralone derivative; Figure 8) in which free rotation of in situ generated C=N double bond was restricted showed a strong band in the long wavelength region corresponding to ESIPT tautomer (Figure 8). The compound **91** which was photoinactive towards cycloaddition reaction but featured a similar chromophore corresponding to *o*-azaxylylene unit showed similar ESIPT band as that of reactive compound **85e** (Figure 8). This indicated that alkenyl tether (dienophile unit) had little or no influence on the nature of ESIPT leading to the formation of the photogenerated tautomer. Based on time correlated single photon counting experiments on **85a** the involvement of triplet excited state during the cycloaddition process was established. The involvement of triplet excited state was further bolstered by quenching experiments with triplet oxygen and piperylene.<sup>83</sup>

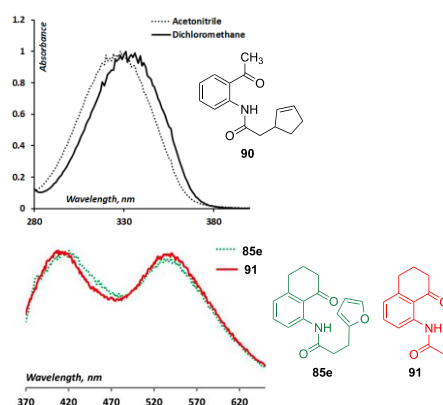
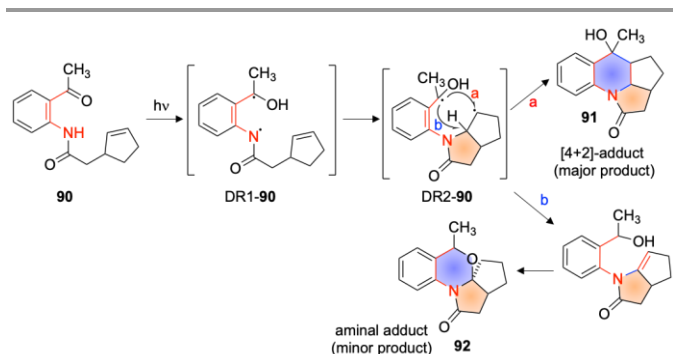


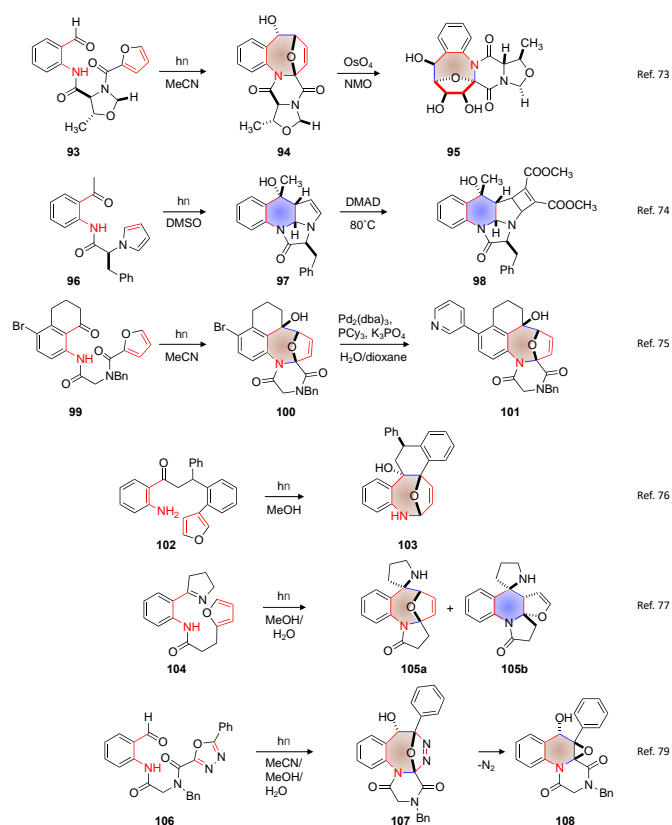
**Figure 8.** UV-Vis absorption spectra of **90** (top) and emission spectra of **85e** and **91** featuring ESIPT band in the longer wavelength region (bottom). Adapted with permission from reference <sup>83</sup> Copyright (2014) American Chemical Society.

Further, Kutateladze and co-workers established that the reaction involved a stepwise mechanism that featured a 1,4-diradical (Scheme 23) in which the nitrogen centred radical of *O*-azaxylylene attacked electron rich dienophile unit followed

by the radical recombination of carbon centred radical to produce product. By investigating the photoactivity of **90** (Scheme 23) they observed the formation of the [4+2]-adduct **91** (route a) and a new product **92** (route b). The formation of **92** was rationalized via a step wise process in the formation of 1,4-diradical DR1-**90**. The initial bond formation was due to the reactivity of the nitrogen centred radical with dienophile unit resulting in DR2-**90**. This diradical DR2-**90** subsequently cyclized to form either the [4+2]-adduct **91** (reaction between carbon centred radical) or undergoes disproportionation followed by cyclization to form **92**.



Scheme 23. Mechanism of ES IPT mediated photocycloaddition of *o*-azaxyllylene.

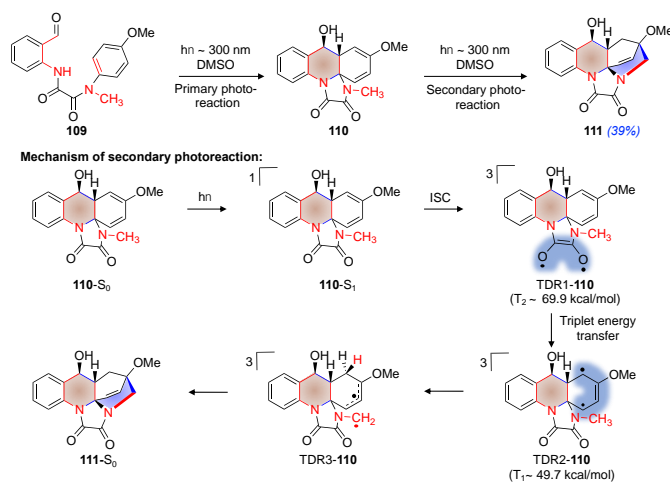


Scheme 24. Application of ES IPT mediated photocycloaddition of in situ generated C=N to build complex structural skeletons.

Kutateladze and co-workers extended their strategy of ES IPT mediated intramolecular photocycloaddition featuring imines for several systems to form polyheterocyclic compounds with

complex structures (Scheme 24).<sup>73–77,79</sup> *o*-Azaxyllylene with suitably tethered pendant group was subjected to photocycloaddition with or without post-photochemical modification to access polyheterocyclic aminoglycosides **95**,<sup>73</sup> enantiopure polyheterocyclic alkaloids **98**,<sup>74</sup> polyheterocyclic biaryls **101**,<sup>75</sup> polyheterocyclic compounds with 2,6-epoxyazocane cores **103**,<sup>76</sup> spiro-polyheterocycles **105a/105b**,<sup>77</sup> and polyheterocyclic ketopiperazine containing spiro-oxirane moiety **108**.<sup>79</sup>

Another interesting reaction reported by Kutateladze and co-workers involved photochemical cascade reaction via in situ generated C=N by ES IPT (Scheme 25).<sup>82</sup> Irradiation of **109** at ~300 nm resulted in the formation of the benzylic alcohol **110** by ES IPT mediated [4+2]-cycloaddition through photogenerated C-N double bond. The primary photoproduct **110** featured *o*-amino phenyl carbonyl unit linked to *N*-methyl-*p*-anisidine through dicarbonyl functionality. Photoexcitation of **110** resulted in a secondary photochemical reaction where an intramolecular hydrogen atom transfer was followed by radical coupling that resulted in the formation of polyheterocyclic product **111** (Scheme 25).<sup>82</sup> They also proposed a mechanistic pathway where an intramolecular energy transfer to low lying T<sub>1</sub> state localized on **110** resulted in the formation of triplet 1,4-diradical TDR1-**110**. This was followed by hydrogen atom tunneling from *N*-methyl group to form diradical TDR2-**110** followed by intramolecular radical coupling to form photoproduct **111** (Scheme 25). Thus, this cascade reaction involved two consecutive photochemical steps to form the final polycyclic product **111** from **109**.

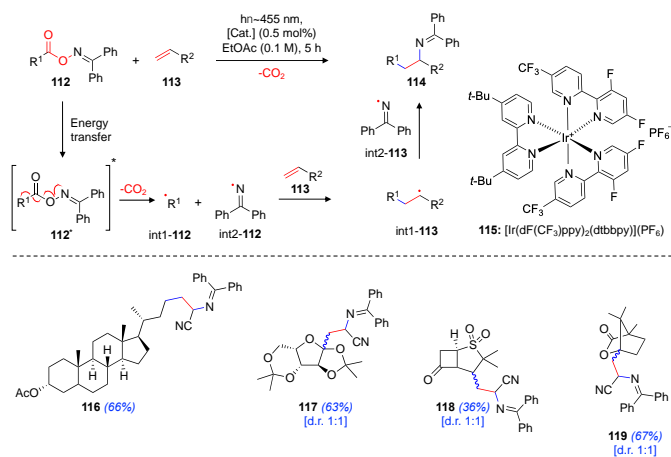


Scheme 25. Cascade photoreaction of oxalylaniide **109** to form polyheterocyclic compound **111**.

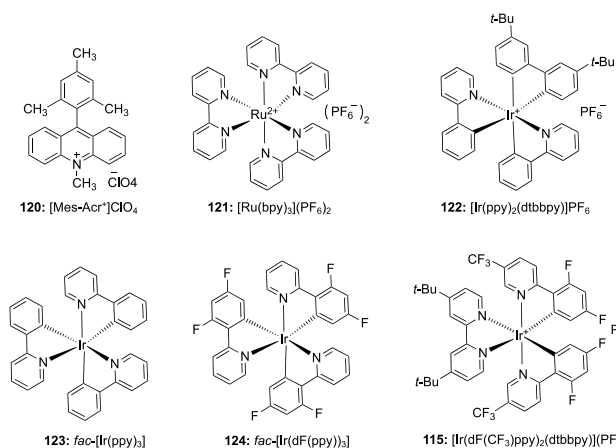
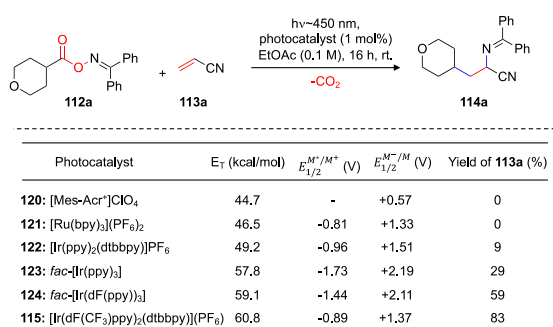
### 3.12 Intermolecular carboimination of imines

Further, Glorius and co-workers<sup>85</sup> reported photochemical inter molecular carboimination of olefins **113** in the presence of oxime esters of benzophenone imine **112** through energy transfer catalysis from photoexcited iridium photocatalyst **115** (Scheme 26). Mechanism involved decarboxylation of photoexcited oxime ester **112\*** by concerted homolytic cleavage of C-C bond and N-O bonds (Scheme 26-top) leading to the formation of carbon centred transient radical int1-**112** and

nitrogen centred persistent radical **int2-112** with the concurrent extrusion of CO<sub>2</sub>. Long lifetime of imine radical resulted in the addition of carbon centred radical to the terminal position of alkene double bond of **112** to generate stable radical **int1-113**. This was followed by persistent radical effect<sup>85,86</sup> where imine radical **int2-112** coupled with **int1-113** to form carboimination product **114** (Scheme 26-top).



**Scheme 26.** Carboimination of imines (top). Carboimination product derived from some natural product carboxylic acids (bottom). The product yields and diastereomeric ratios are provided in parenthesis.

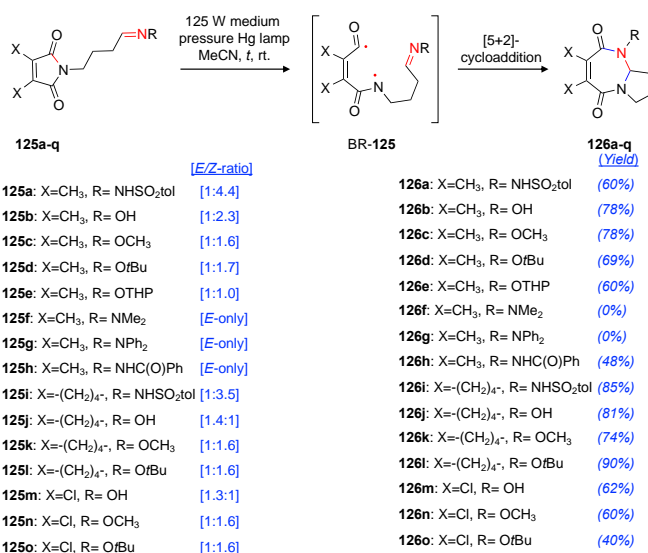


**Scheme 27.** Effect of triplet energy of photocatalyst on carboimination of olefin **113a** with benzophenone oxime ester **112a**.

Carboimination strategy showed wide range of substrate scope with oxime esters derived from substituted aliphatic carboxylic acid that generated primary, secondary or tertiary carbon centred radical **int1-112** upon photodecarboxylation.

Alkene double bond of **113** with electron withdrawing group or phenyl substituent at  $\alpha$ -position was quite efficient in the reaction. Reaction showed high functional group tolerance and can be extended to natural products containing carboxylic acids such as lithocholic acid, diprogolic acid, sulbactam and 1S(-)-camphanic acid to form the corresponding carboimination product **116**, **117**, **118** and **119** (Scheme 26-bottom) respectively, with moderate to good yield.

Further, Glorious and co-workers demonstrated that the yield of carboimination product **114a** with oxime ester **112a** (that had triplet energy,  $E_{T(112a)} \sim 45.4$  kcal/mol) increased with increasing triplet energy of photocatalyst (Scheme 27) indicating that the reaction involved energy transfer pathway. Electron transfer pathway by reductive quenching was discounted, as maximum yield was not observed with highly reducing photocatalyst (Scheme 27, **123:** fac-[Ir(ppy)<sub>3</sub>],  $E_{1/2}^{M^*/M} = +2.19$  V). Similarly single electron transfer by oxidative quenching was also disregarded as no product was formed with highly oxidizing photocatalyst (**120:** [Mes-Acr<sup>+</sup>ClO<sub>4</sub>],  $E_{1/2}^{M^*/M} = +2.06$  V).<sup>85</sup>

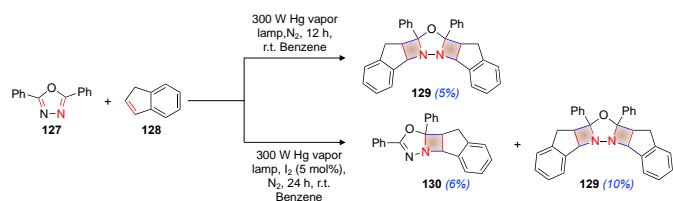


**Scheme 28.** [5+2]-photocycloaddition of imine double bond. The product yields and E/Z ratios of imine are provided in parenthesis.

### 3.13 Higher order photocycloaddition of involving imines

Booker-Milburn and co-workers<sup>87</sup> reported intramolecular [5+2]-photocycloaddition of imine double bond tethered to maleimide chromophore **125a-e**, **125h-o** to form 1,3-diazepine derivatives **126a-e**, **126h-o** (Scheme 28). Reaction involved homolysis of C-N single bond of maleimide unit to form biradical BR-125 that added to the imine double bond to form [5+2]-cycloadduct **126** (Scheme 28). Reactive imines **125a-e**, **125h-o** possessed electron deficient imine double bond that was a part of hydrazones or oximes tether featuring a mixture of E/Z isomers (except **125h** which featured exclusively in E-isomer). However unreactive N,N-dimethylhydrazine imine **125f** and N,N-diphenyl hydrazine imine **125g** had relatively electron rich imine double bond and possessed only E-isomer. This indicated that photocycloaddition was favoured with electron deficient

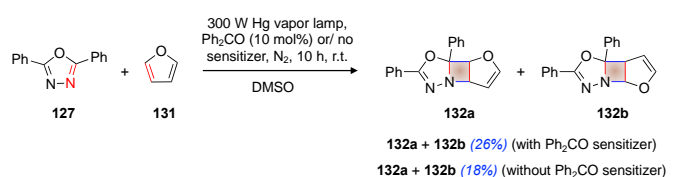
imines consisting of Z-isomer. Reaction showed highest quantum yield at the wavelength corresponding to  $n \rightarrow \pi^*$  transition (e.g.  $\Phi = 0.12$  at 310 nm for the formation of **126c**) indicating that reactive imines possessed  $n \rightarrow \pi^*$  excited state localized on maleimide chromophore. Singlet mechanism was proposed as the reaction was unaffected by the presence of triplet quencher piperylene.



**Scheme 29.** Photocycloaddition of imine double bond of 2,5-diphenyl-1,3,4-oxadiazole with indene. (The product yields are provided in parenthesis).

#### 4. [2+2]-photocycloaddition of cyclic imines

Unlike well-known Paternò-Büchi reaction,<sup>88–91</sup> where excited carbonyl group undergoes [2+2]-photocycloaddition with the alkene double bond to form oxetane ring, corresponding reaction of imine double bond, i.e. addition of excited carbon-nitrogen double bond to the ground state alkene double bond to form azetidene ring is not extensively reported.<sup>4,5</sup> The challenges associated with [2+2]-photocycloaddition of imine double bond is due to several relaxation/reaction pathways possible for the excited imine as detailed in the previous sections (Sections 2 and 3). Among them, *E-Z* isomerization is one of the common pathways for the relaxation of excited imine to its ground state.<sup>4,5</sup> A simple strategy to avoid *E-Z* isomerization, and there by restrict the deactivation of the excited state is to tether the imine double bond as part of a cyclic system. This strategy was implemented successfully for [2+2]-photocycloaddition of excited imine featuring cyclic structure.<sup>92–98</sup>

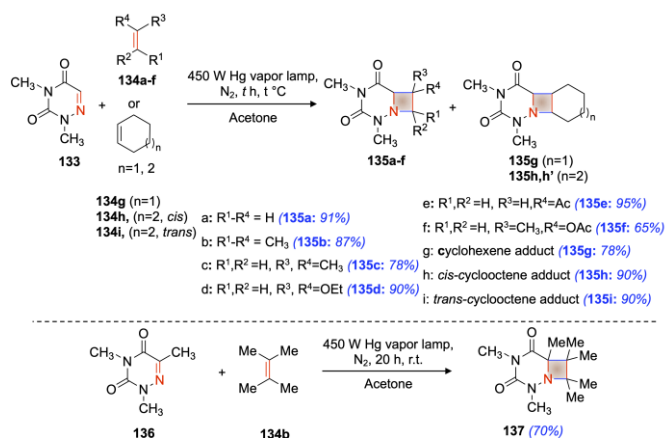


**Scheme 30.** [2+2]-photocycloaddition of C-N double bond of 2,5-diphenyl-1,3,4-oxadiazole with furan. The product yields are provided in parenthesis.

In 1968 Tsuge and co-workers<sup>92</sup> reported the first photocycloaddition of excited imine double bond to an ground state alkene (Scheme 29). Irradiation of solution of 2,5-diphenyl-1,3,4-oxadiazole **127** and indene **128** in benzene in the presence of 5 mol% iodine with high pressure mercury lamp resulted in the formation of 1:1 adduct **130** (where photocycloaddition occurred on one of the imine double bonds in **127**) and 1:2 adduct **129** (where both the imine double bonds in **127** underwent photocycloaddition). In the absence of iodine only the 1:2 adduct **129** was formed.

Tsuge and co-workers<sup>93</sup> also reported photocycloaddition of 2,5-diphenyl-1,3,4-oxadiazole **127** with furan **131** to form regioisomeric mixture of 1:1 adduct of **132a** and **132b** with 18% yield (Scheme 30). In the presence of benzophenone sensitizer, the yield of photoproduct was increased to 26% (for the mixture) (Scheme 30). In the presence of triplet quencher piperylene, no photoproduct was formed indicating that photocycloaddition involved triplet excited state of **127**.

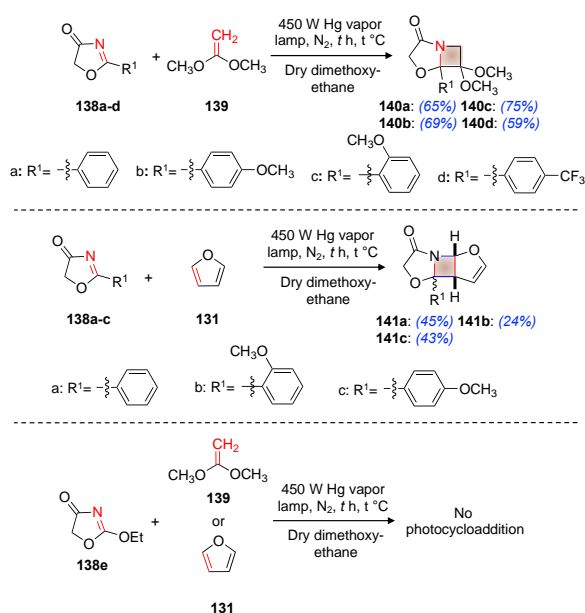
Swenton and co-workers<sup>96,97,99</sup> reported acetone sensitized photocycloaddition of 1,3-dimethyl-6-azathymine **133** with acyclic alkenes **134a-f** and cyclic alkenes **134g-i** to form the corresponding azetidene product **135** (Scheme 31-top). Regioselective addition was observed with unsymmetrical alkenes where nitrogen atom of major product was attached to the more substituted carbon atom of alkene double bond.<sup>97</sup> Photoproduct was observed in moderate to excellent isolated yields (65–90%). Similarly, 1,3-dimethyl-6-azauracil **136** reacted with tetramethyl ethylene **134b** to form the corresponding azetidene product **137** with an isolated yield of 70% (Scheme 31-bottom).<sup>97</sup>



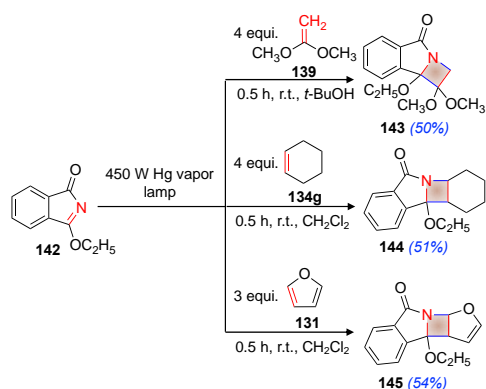
**Scheme 31.** [2+2]-Photocycloaddition of 1,3-dimethyl-6-azathymine (top) and 1,3-dimethyl-6-azauracil (bottom) with alkenes. The product yields are provided in parenthesis.

Koch and co-workers<sup>100</sup> reported [2+2]-photocycloaddition of 2-oxazoline-4-one derivative **138a-d** and 1,1-dimethoxy ethene **139** to form azetidene derivative **140a-d** (Scheme 32-top). Reaction was efficient with oxazoline derivatives **138b** and **138c** that had electron rich methoxy substituents on the phenyl ring conjugated to imine double bond. Electron deficient oxazoline derivative **138d** and unsubstituted phenyl derivative **138a** gave lower yields of photoproduct. Irradiation of oxazoline derivatives **138a-c** with furan **131** resulted in the regioselective cycloaddition to form azetidene derivative **141a-c** (Scheme 32-middle) with low to moderate yields.<sup>100</sup> However, 2-ethoxy-2-oxazoline-4-one **138e** failed to undergo photocycloaddition under similar conditions (Scheme 32-bottom).<sup>100</sup> Instead, 2-ethoxy-2-oxazoline-4-one **138e** upon photoirradiation resulted in  $\alpha$ -cleavage, a reaction characteristic of  $n\pi^*$  excited state of ketones. However, UV-Vis spectra of reactive oxazoline derivative **138b** and **138c** featured intense  $\pi\pi^*$  band. It was hypothesised that reactive oxazoline derivative had imine

double bond featuring lowest  $\pi\pi^*$  excited state, due to stabilization from electron donating group/extended conjugation in aryl substituted oxazoline derivatives **138a-d**.<sup>100</sup>

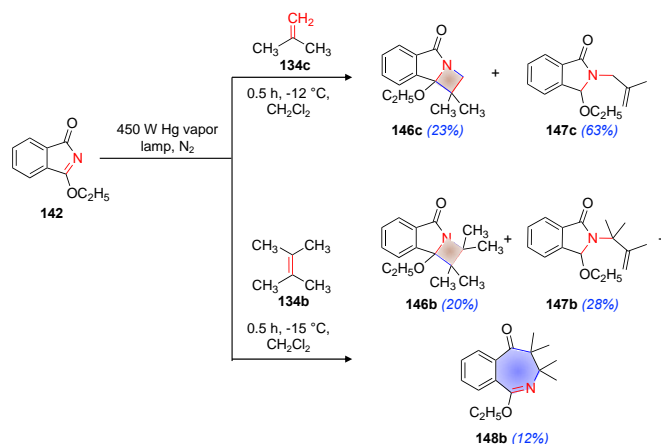


**Scheme 32.** [2+2]-photocycloaddition of 2-oxazoline-4-one derivative with alkene double bond. The product yields are provided in parenthesis.

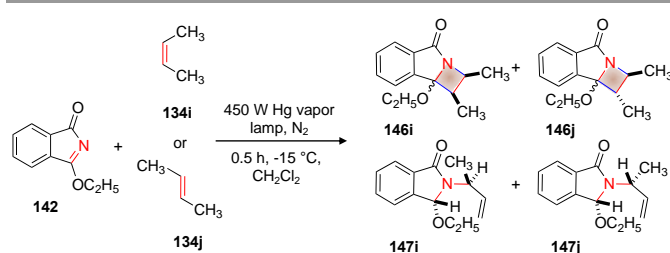


**Scheme 33.** [2+2]-photocycloaddition of 3-ethoxyisoindolone with alkene double bond. (The product yields are provided in parenthesis).

Koch and co-workers reported [2+2]-photocycloaddition of imine double bond of 3-ethoxyisoindolone **142** with alkene double bond (Scheme 33, 34).<sup>94,95</sup> Benzo group in 3-ethoxyisoindolone **142** reduced the tendency for  $\alpha$ -cleavage<sup>55,100</sup> and stabilized of  $\pi\pi^*$  excited state localized on imine double bond by conjugation, hence facilitating imine-alkene photocycloaddition. Photoirradiation of 3-ethoxyisoindolone **142** with 1,1-dimethoxyethene **139**, cyclohexene **134g** and furan **131** resulted in the formation of corresponding azetidine derivatives **143**, **144** and **145** respectively, with moderate yields (Scheme 33).<sup>95</sup> Regioselective photocycloaddition was observed with 1,1-dimethoxyethene **139** and furan **131** (Scheme 33).



**Scheme 34:** Photoreaction of 3-ethoxyisoindolone with alkene. The product yields are provided in parenthesis.



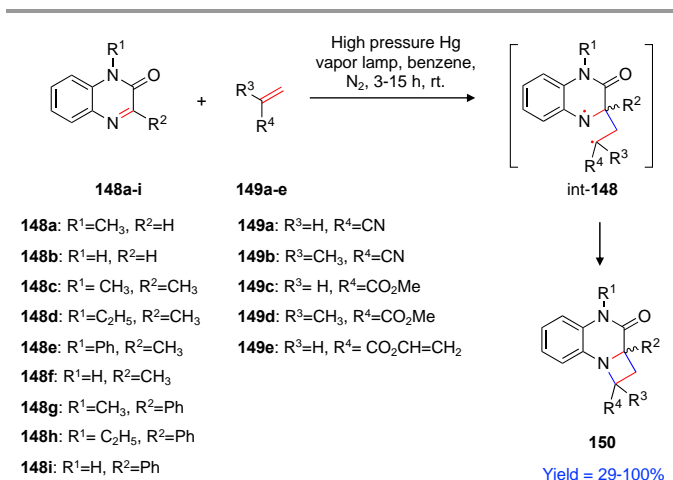
**Scheme 35.** Photoreaction of 3-ethoxyisoindolone with *cis/trans*-2-butene.

**Table 3.** Product distribution in the photoreaction of 3-ethoxyisoindolone with *cis/trans*-2-butene.

Olefin	[ <b>134</b> ] mol/L	[ <b>146i</b> ]/ [ <b>146j</b> ]	[ <b>147i</b> ]/ [ <b>147j</b> ]	[ <b>146i</b> ]/[ <b>146j</b> ]/ [ <b>147i</b> ]/[ <b>147j</b> ]
<b>134i</b> : <i>cis</i> -2-Butene	0.92	2.0	3.10	0.72
<b>134i</b> : <i>cis</i> -2-Butene	0.37	2.1	2.90	0.73
<b>134j</b> : <i>trans</i> -2-Butene	0.92	2.1	0.69	1.70
<b>134j</b> : <i>trans</i> -2-Butene	0.37	2.0	0.37	1.80

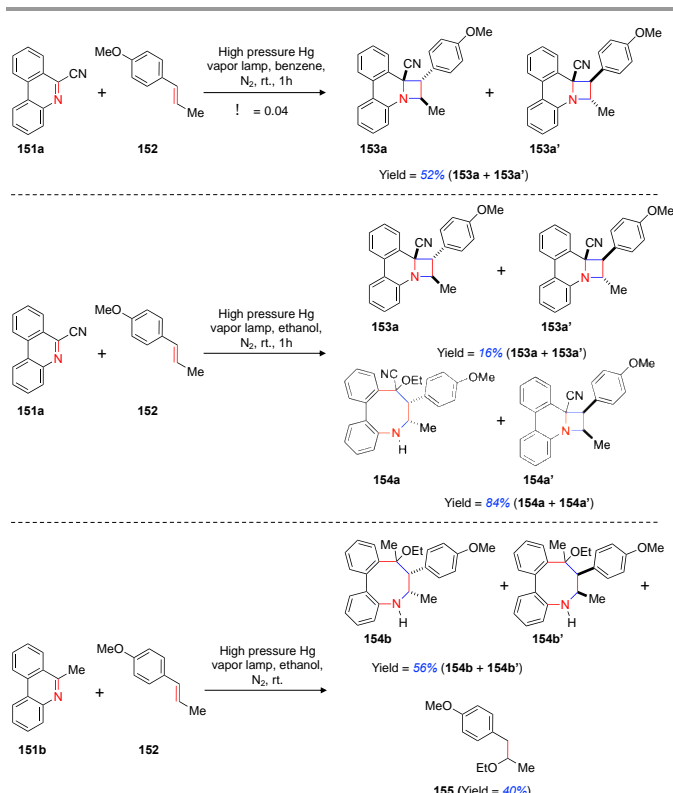
Photoreaction of 3-ethoxyisoindolone **142** with isobutylene **134c** resulted in a major product **147c** in 63% yield and a minor product **146c** in 23% yield (Scheme 34-top).<sup>95</sup> However, photoirradiation of 3-ethoxyisoindolone **142** in the presence of tetramethyl ethylene **134b** resulted in the formation of a new photoproduct benzoazepinone derivative **148b** in addition to **146b** and **147b** and (Scheme 34-bottom).<sup>95</sup> The reaction was postulated to proceed via a triplet diradical intermediate. In addition, the alkenes were found to quench the excited singlet state of **142**. The involvement of a triplet diradical in the reaction pathway was confirmed by alkene scrambling studies. Photoreaction of 3-ethoxyisoindolone **142** with *cis*-2-butene **134i** or *trans*-2-butene **134j** resulted in the formation mixture of cycloaddition products **146i/146j** as well as **147i/147j** (Scheme 35).<sup>95</sup> Complete scrambling of stereochemistry of cycloadduct diastereomers **146i/146j** was observed (Table 3, column 3). This observation substantiated long lived 1,4-diradical mechanism for the formation of cycloadduct (Scheme 34, bottom).<sup>95</sup> A slight diastereomeric preference for one of the

ene-product (Table 3; 4<sup>th</sup> column) that was rationalized based on the formation of a triplet exciplex which restricted C-C bond rotation of alkene moiety reflecting in the observed diastereoselectivity.



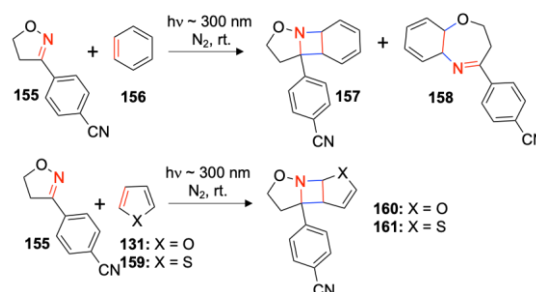
**Scheme 36.** [2+2]-photocycloaddition of C-N double bond of quinoxaline-2(1H)-one to alkene double bond.

Nishio<sup>101</sup> reported [2+2]-photocycloaddition of imine double bond of quinoxaline-2(1H)-one **148a-i** with electron deficient alkene **149a-e** to form azetidine derivative **150** (Scheme 36). Reaction followed regioselective addition where imine nitrogen attached to the internal-carbon of alkene moiety in the azetidine product. Triplet mechanism was proposed for the observed photochemical reactivity.



**Scheme 37.** [2+2]-photocycloaddition of C-N double bond of 6-cyanophenanthridine.

Ohta and co-workers<sup>102,103</sup> reported [2+2]-photocycloaddition of 6-cyanophenanthridine **151a** with *trans*-anethole **152** in benzene. Diastereomeric mixture of [2+2]-photoadduct **153a**, **153a'** was formed in 52% isolated yield with a quantum yield of 0.04 (Scheme 37-top).<sup>102</sup> However, when the same reaction was performed in a polar solvent – ethanol, in addition to [2+2]-photoadduct **153a**, **153a'**, azocine derivatives **154a**, **154a'** was also formed (Scheme 37-middle).<sup>103</sup> Irradiation of 6-methylphenanthridine **151b** and *trans*-anethole **152** in ethanol resulted in the formation azocine derivative **154b**, **154b'** and **155** (Scheme 37-bottom) but the [2+2]-photoproduct was not observed.<sup>103</sup> They also observed that 6-methylphenanthridine **151b** failed to undergo photocycloaddition with **152** in benzene. Similarly, *cis*-anethole did not react with **151a** or **151b**. Based on photophysical investigations the observed reactivity was rationalized through the formation of an exciplex. This conjecture was substantiated by quenching of **151a** fluorescence with *trans*-anethole with the concurrent formation of new emission at longer wavelength corresponding to exciplex of [**151a...152**]\*. Formation of azocine derivative **154b**, **154b'** and **155** (Scheme 37-middle, bottom) substantiated the exciplex mechanism resulting in the formation radical cation of **154** or **152** followed by the nucleophilic addition of ethanol. Triplet quencher *trans*-1,3-butadiene failed to quench the reaction during photocycloaddition, negating the involvement of the triplet excited state. In addition, the reaction featured a ππ\* excited state of phenanthridine **151a,b** in ethanol with a the longer lifetime that enabled exciplex formation with *trans*-anethole **152** facilitating the formation of corresponding product(s).



**Scheme 38.** [2+2]-photocycloaddition of CN double bond of 3-(*p*-cyanophenyl)-2-isooxazoline derivatives.

Mukai and co-workers reported [2+2]-photocycloaddition of C-N double bond of 3-(*p*-cyanophenyl)-2-isooxazoline with benzene **155**,<sup>98,104</sup> furan **131** or thiophene **159**<sup>105</sup> to form corresponding azetidine derivatives **157**, **160** and **161** respectively (Scheme 38). Photoreaction of **155** with benzene **156** also resulted in the addition across N-O bond to form **158** (Scheme 38-top). Reaction involved singlet state 3-(*p*-cyanophenyl)-2-isooxazoline as it showed fluorescence quenching in the presence of benzene. However, 3-phenyl-2-isooxazoline without electron withdrawing group on the phenyl ring failed to undergo cycloaddition.<sup>98</sup> Later Sampedro and co-workers<sup>106,107</sup> explored computational analysis for [2+2]-photocycloaddition of 2-isooxazolines (Chart 1). Computational analysis predicted that imine photocycloaddition competes

with fast deactivation of excited state. As per their observation, cyclic imine requires some additional structural features for facile photocycloaddition to C=N. This could be achieved with electron withdrawing groups attached to imine nitrogen or to any part of molecule which can induce electron withdrawing inductive effect on imine moiety. Among the compound in Chart 1 isoxazoline **163** has more electron deficient imine nitrogen compared to pyrroline **162**. Similarly, imine nitrogen of 3-(*p*-cyanophenyl)-2-isooxazoline **155** is more electron deficient compared to that in 3-phenyl-2-isooxazoline **164** (Chart 1). Their computational investigation revealed that low energy conical intersections led to faster deactivation while high energy conical intersection enabled the photocycloaddition to occur as the molecule could spend more time in the excited state. This was demonstrated with the irradiation of isooxazoline imine with electron withdrawing cyano group **165** in the presence of furan **131** that resulted in regioselective [2+2]-photocycloaddition to form diastereomeric mixture **166a**, **166b** (Scheme 39).<sup>107</sup> In the absence of cyano group in the imine moiety, photocycloaddition was not observed.

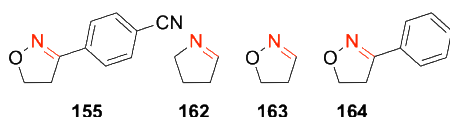
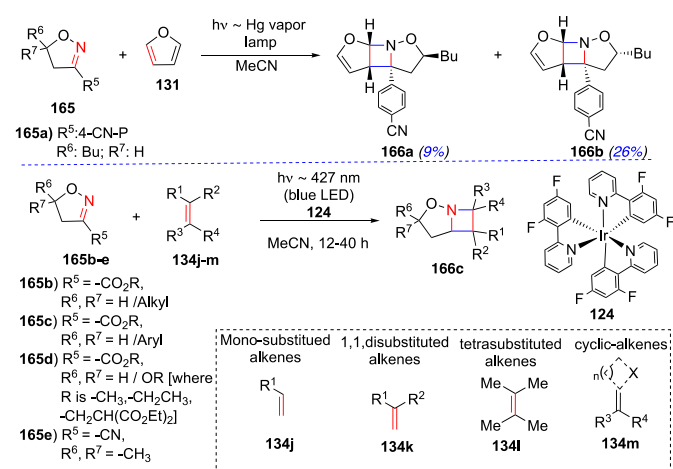


Chart 1. Cyclic imines with and without electron withdrawing group.



Scheme 39. [2+2]-Cycloaddition of photoexcited C-N double bond in isooxazoline derivatives.

Schindler and co-workers<sup>108</sup> reported the intermolecular [2+2] photocycloadditions involving 2-isooxazoline-3-carboxylates derivatives **165b-e** with alkenes **134j-m** leading to the corresponding azetidines photoproduct **166c** (Scheme 39-bottom). The reaction was performed under energy transfer conditions with iridium photocatalyst **124**. The reaction was effective for electron withdrawing group ( $R^5$ ) in **165b** such as carboxylates and cyanide. The reaction involved generation of a triplet excited C-N double bond (via triplet energy transfer). A triplet excited C-N double bond was part of a cyclic system and it efficiently added to both linear and cyclic alkenes leading to the corresponding azetidines photoproduct **166c**.<sup>108</sup>

## 5. Recent developments on [2+2]-photocycloaddition of C-N double bond – Reactions involving acyclic imines.

As detailed in the section 4, earlier reports involving [2+2]-photocycloaddition of C-N double bond featured cyclic imines to prevent their facile photo-induced isomerization. This limited the substrate scope of the reaction. Only cyclic imines featuring electron withdrawing groups or cyclic imines that are part of a conjugated system were employed to direct the photocycloaddition to the imine double bond limiting its wide spread applicability (Figure 9-top).<sup>4,5</sup>

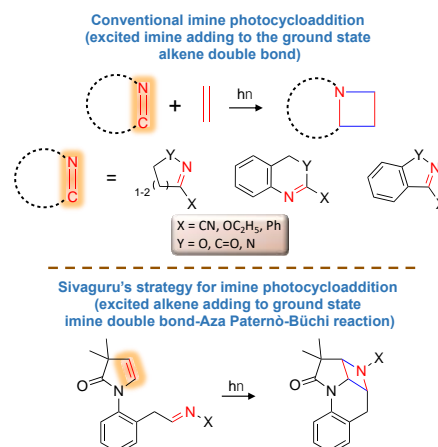
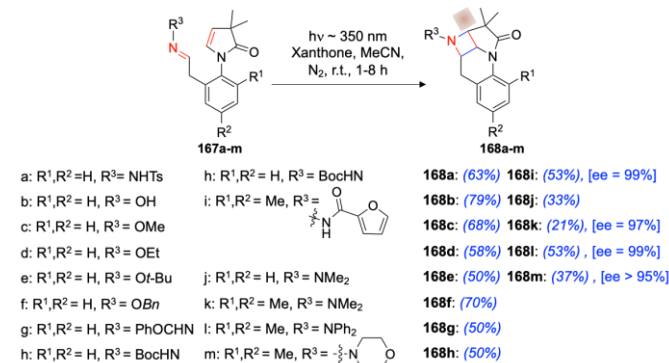


Figure 9. Various strategies for [2+2]-photocycloaddition of C-N double bond to alkene double bond.

Sivaguru and co-workers developed a new strategy for intramolecular [2+2]-photocycloaddition of acyclic imine double bond with alkene double bond called Aza Paternò-Büchi reaction.<sup>109</sup> This opened up a new avenue for imine photocycloaddition involving acyclic imines, broadening the scope of this reaction. In this strategy, alkene double bond was excited (instead of imine double bond as in the earlier reports - section 4) to access azetidines products. This avoids undesirable reactions/relaxation pathways associated with imine excitation (sections 2 and 3) enabling ground state imine double bond to add to an excited alkene double bond (Figure 9-bottom).



Scheme 40. Strategy for Aza Paternò-Büchi reaction developed by Sivaguru and co-workers<sup>109</sup> utilizing of imine **167a-m** to form corresponding azetidines derivatives **168a-m**. The product yields are provided in parenthesis. ee: enantiomeric excess.

To showcase the above strategy, *N*-phenyl enamide derivative featuring an imine tether **167** (Scheme 40)<sup>109</sup> was excited by triplet sensitization with xanthone ( $E_T=74$  kcal/mol) acting as a photocatalyst/sensitizer (Scheme 40). Photosensitization resulted in alkene excitation that reacted with ground state imine to form the azetidine photoproduct. This addition C=C to C=N bond was named as the “Aza Paternò-Büchi reaction”. The strategy was found to be quite general as it was employed for reactivity of stabilized imine (Scheme 40 - tosylate **167a**, oximes **167b-f**, hydrazones **167h-i** where imine nitrogen attached to electron withdrawing group) as well as non-stabilized imines (hydrazides **167j-m**). The strategy yielded moderate to good isolated yields (21-79%) of the azetidine photoproduct. The reaction was also extend to atropisomeric substrates **167i**, **167k-m** (Scheme 40; where  $R_1, R_2 = CH_3$ ) resulting in excellent atropselectivity/enantioselectivity ( $ee=95-99\%$ ) in the azetidine photoproduct.<sup>109</sup>

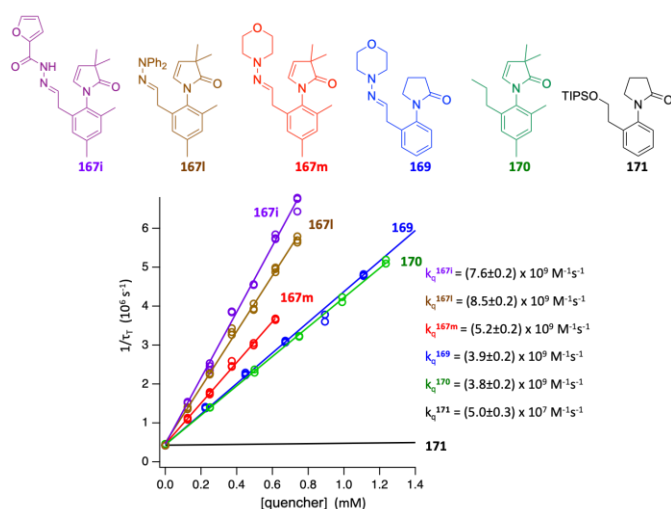
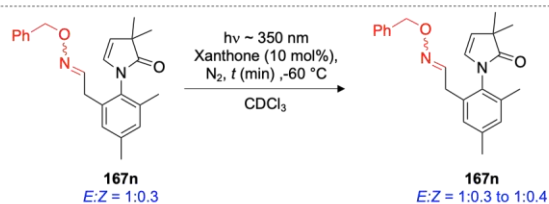
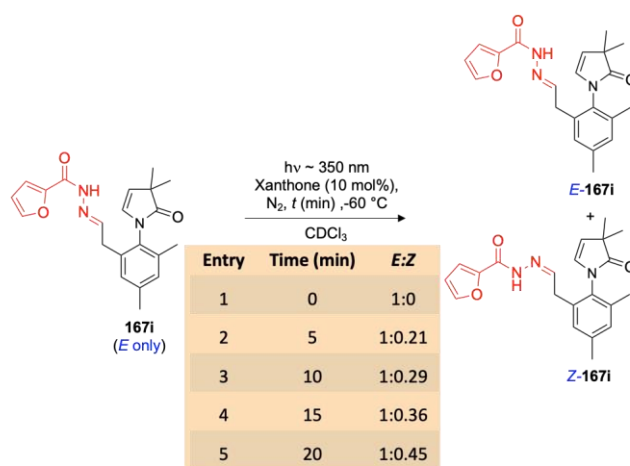


Figure 10. Determination of quenching rate constant for the quenching of xanthone triplets with different substrates.

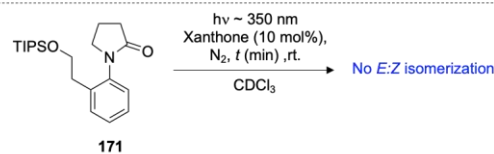
To understand the novel excited state reactivity involving imines leading to Aza Paternò-Büchi reaction, Sivaguru and co-workers performed detailed photophysical investigations (Figure 10) that revealed the excitation of alkene double bond of enamide chromophore initiated the cycloaddition with ground state imine double bond. Bimolecular quenching rate constant ( $k_q$ ) of the xanthone triplets with enamide-imines revealed the mechanistic intricacies of Aza Paternò-Büchi reaction (Figure 10). Enamide **170** that lacked the imine functionality gave  $k_q$  of  $3.8 \pm 0.2 \times 10^9 M^{-1}s^{-1}$ . This indicated that the alkene is excited through triplet energy transfer. Imine **169** that lacked the enamide but featured a tertiary amine gave  $k_q$  of  $3.9 \pm 0.2 \times 10^9 M^{-1}s^{-1}$  indicating an electron transfer mediated quenching of xanthone triplet excite state. Substrates featuring both the enamide and imine functionalities (**167i**, **167l-m**) quenched the excited xanthone triplets with quenching constants close to diffusion control rates. The bimolecular quenching rate constants was two order lower for amide **171** that lacked both the imine and alkene double bounds. The photophysical investigation clearly established that the alkene

part of the enamide was excited by triplet energy transfer from photoexcited xanthone (Figure 10).

To further establish the role of the excited alkene double bond in Aza Paternò-Büchi reaction, control studies were carried out with enamide-imines **167i** and **167n** imine **169** (Scheme 41). Enamide-imine **167i** that exist exclusively as *E*-isomer at room temperature (confirmed by <sup>1</sup>H-NMR spectroscopy) was subjected to low temperature irradiation (Scheme 41-top). Xanthone sensitization at  $-60$  °C in  $CDCl_3$  showed the formation of the *Z*-isomer during the course of reaction. Enamide-imine **167n** that exists as a mixture of *E/Z* isomers was subjected to similar low temperature irradiation studies (Scheme 41-middle). The reactivity of **167n** revealed that the *E*-isomer reacted faster than the corresponding *Z*-isomer that was reflected in the *E/Z* ratio. However, imine **169** that lacked enamide functionality did not undergo *E/Z* isomerization upon xanthone sensitized irradiation (Scheme 41-bottom). This indicated that the energy transfer happened from the excited sensitizer to enamide-motif in **167** followed by formation of a transient species that scrambles the imine geometry. The variation of *E/Z* ratio reflected the different rate of reaction of *E* and *Z* isomer.



Entry	Time (min)	% Conversion	E:Z
1	0	-	1:30
2	5	9	1:0.36
3	10	16	1:0.38



Scheme 41. Mechanistic investigation to decipher intricacies of Aza Paternò-Büchi reaction.

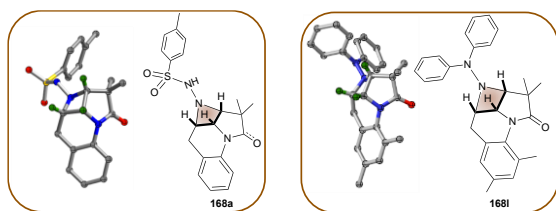
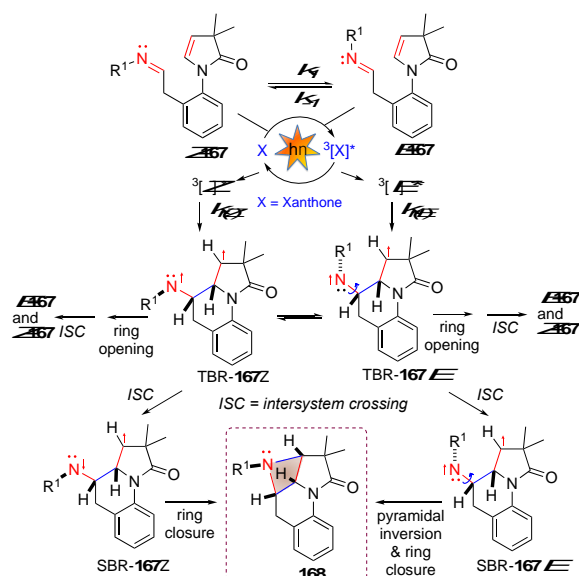


Figure 11. XRD structure of photoproduct **168a** (formed from *E/Z* mixture of imine **167a**) and **168l** (formed from pure *E* imine **167l**).

XRD structure of photoproduct **168a** and **168l** (Figure 11) revealed that photoreaction of imine with mixture of *E/Z* isomers (such as **167a**, *E/Z* ratio = 1:5.5) or imine with only *E* isomer (such as **167l**) resulted in single stereoisomeric product in which all the hydrogen at the azetidine ring are *syn* to each other. This indicated that the reaction mechanism involved a common intermediate irrespective of whether reaction originated from *E* or *E/Z*-mixture of **167** eventually leading to the formation of azetidine photoproduct.

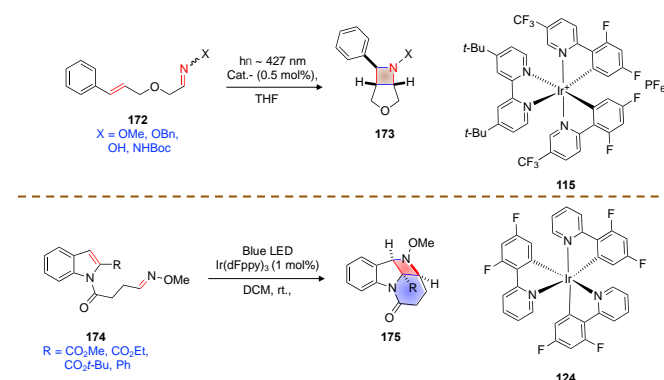
Based on detailed photophysical investigation, mechanism for formation of azetidine was proposed (Scheme 42). The enamide-imine *E/Z* ratio (ascertained by  $^1\text{H-NMR}$  spectroscopy) in the ground depended on its thermodynamic stability. Upon sensitized irradiation with xanthone, both *E* and *Z* imine formed the corresponding 1,4-triplet biradical TBR-**167E** and TBR-**167Z**, respectively. These triplet biradical intersystem crossed to the corresponding singlet biradical SBR-**167E** and SBR-**167Z**, respectively. The singlet biradical underwent cyclization to form azetidine photoproduct **168**. Based on the XRD structure (Figure 11) that shows *syn*-orientation of the cyclobutyl-hydrogens and  $\text{N-R}^1$  substituent is either a reflection of differential reactivity of the equilibrated diradicals and/or pyramidal inversion on the nitrogen center to form the stable azetidine product.



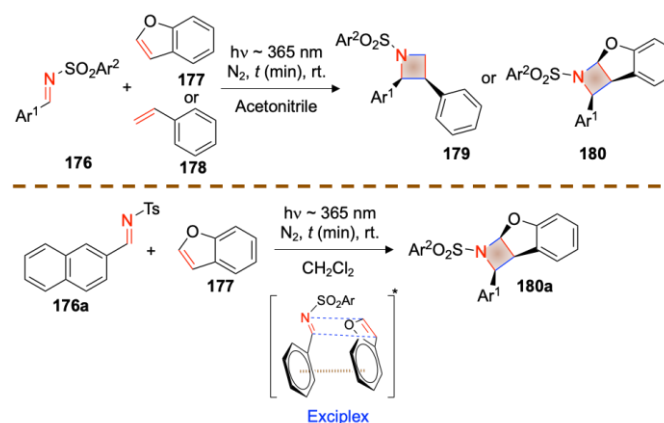
Scheme 42. Proposed mechanism of Aza-Paternò-Büchi reaction.

Based on Sivaguru's methodology (Schemes 40-42), Schindler and co-workers<sup>110</sup> reported the aza-Paternò-Büchi reaction of acyclic imines **172** in the presence of iridium catalyst

**115** as a triplet sensitizer to form corresponding azetidine derivatives **173** (Scheme 43-top). Similar to the enamide-imine reactivity, triplet energy transfer from photoexcited iridium **115** resulted in triplet excited styrenyl functionality, followed by addition to the imine double bond resulting in the azetidine product **173** (Scheme 43-top). You and co-workers<sup>111</sup> also employed Sivaguru's methodology for intramolecular [2+2]-photocycloaddition of *N*-tethered indole oximes to form corresponding azetidine derivatives (Scheme 43-bottom). Photoirradiation of imine **174** in the presence triplet sensitizer Ir(dFppy)<sub>3</sub> **124** resulted in the excitation of indole alkene double bond by triplet energy transfer from sensitizer, which then added to the imine double bond resulting in the formation azetidine derivative **175** (Scheme 43-bottom).



Scheme 43. Aza Paternò-Büchi reaction of imine **172** by triplet sensitization by Schindler and co-workers<sup>110</sup> (top) and You and co-workers<sup>111</sup> (bottom)



Scheme 44. Strategies for aza Paternò-Büchi reaction of acyclic imines developed by Maruoka and co-workers.

Maruoka and co-workers<sup>112</sup> reported a different strategy in which photoexcited imine double bond of *N*-tosyl aryl imine **176** added to C-C double bond of benzofuran **177** or styrene **178** to form azetidines (Scheme 44). The reaction was postulated to occur through a singlet exciplex as the *syn*-isomer of azetidine photoproduct was observed exclusively. The observation of a single isomer was rationalized to rule out the triplet pathway. The proposed mechanism involved the formation of singlet state exciplex by that locks the stereochemistry of the azetidine product leading to the formation of single isomer (*syn*-azetidine **179**, **180**). However, the reaction involved some constraints

with respect to the choice of substrate such as a) only protected imines were effective in the reaction; and b) imine with protecting group other than tosyl group (such as boc protected imine) did not afford any product.

## 6.0 Outlook

The immense potential of utilizing the excited state characteristics of imines to uncover new reactivity will undoubtedly drive new research directions by offering complementary reactivity to the well-established photochemistry of carbonyl compounds.<sup>6</sup> This necessitates a thorough understanding of the excited state properties of to tailor their reactivity for applications in synthesis<sup>4,5,72–82</sup> and materials chemistry.<sup>27,29,30,36</sup> Initial investigations in literature focused addressing the multitude of side reactions that occur upon photoexcitation of imines. This was addressed in part by employing cyclic imines to overcome their inherent photoreactivity. Recent developments have showcased how one can utilize acyclic imines in photochemical reactions.<sup>109</sup> The rich and diverse photochemistry and photophysics of imines offers a fertile playground to investigate new excited state transformations.

## 7.0 Conclusions

The review showcases the rich photochemical and photophysical diversity of imines. Understanding the excited state features of imines would help in channelling their unique features to control photochemical and photophysical events. Various reactivity of imine double bond are detailed in this review. These include hydrogen abstraction, cleavage reaction, electron transfer, photoreduction, photofragmentation, photo oxidation, photorearrangement, photohydrolysis, ring expansion, ESIPT mediated photocycloaddition, photochromism and [2+2]-photocycloaddition. In addition, review also details how one can control the reactivity involving imine double bond by bypassing imine excitation, instead of exclusively exciting the alkene counterpart. These aspects will undoubtedly open up new avenues to utilize the unique excited state properties of imines to build complex structural skeletons<sup>73,74,76–80,82</sup> and to access novel materials with tailored properties.<sup>27,29,30,36</sup>

## Conflicts of interest

“There are no conflicts to declare”.

## Acknowledgements

The authors thank the generous support from the National Science Foundation (CHE-1955524) and BGSU. SK and SA thank the McMaster Fellowship (2018-2019 for SK and 2019-2020 for SA) from the Centre for Photochemical Sciences. Authors thank Dr. Ravichandranath Singathi and Ms. Sruthy Baburaj for their valuable suggestions during the preparation of this review.

## Dedication

The authors dedicate this review to Prof. K. K. Balasubramanian, Professor emeritus, Indian Institute of Technology, Madars on the occasion of his 80<sup>th</sup> birthday. Prof. Balasubramanian is an inspiring mentor who has motivated scholars around the world with his research and teaching.

## ORCID

Sunil Kandappa: [0000-0002-6750-4778](https://orcid.org/0000-0002-6750-4778)

Sapna Ahuja: [0000-0002-3060-9699](https://orcid.org/0000-0002-3060-9699)

Lakshmy Kannadi Valloli: [0000-0003-1836-5916](https://orcid.org/0000-0003-1836-5916)

Jayachandran Parthiban: [0000-0002-5916-1701](https://orcid.org/0000-0002-5916-1701)

Jayaraman Sivaguru: [0000-0002-0446-6903](https://orcid.org/0000-0002-0446-6903)

## Notes and references

- 1 R. W. Layer, *Chem. Rev.*, 1963, **63**, 489–510.
- 2 T. Vilaivan, W. Bhanthumnavin and Y. Sritana-Anant, *Curr. Org. Chem.*, 2005, **9**, 1315–1392.
- 3 S. F. Martin, *Pure Appl. Chem.*, 2009, **81**, 195–204.
- 4 A. Padwa, *Chem. Rev.*, 1977, **77**, 37–68.
- 5 A. C. Pratt, *Chem. Soc. Rev.*, 1977, **6**, 63–81.
- 6 N. J. Turro, V. Ramamurthy and J. C. Scaiano, *Modern Molecular Photochemistry of Organic Molecules*, University Science Books, 2010; pp 629–704.
- 7 A. D. Richardson, M. R. Becker and C. S. Schindler, *Chem. Sci.*, 2020, **11**, 7553–7561.
- 8 D. Uruguchi, Y. Tsuchiya, T. Ohtani, T. Enomoto, S. Masaoka, D. Yokogawa and T. Ooi, *Angew. Chem. Int. Ed.*, 2020, **59**, 3665–3670.
- 9 Y.-Q. Zou, F. M. Hörmann and T. Bach, *Chem. Soc. Rev.*, 2018, **47**, 278–290.
- 10 J. D. Coyle, *Introduction to Organic Photochemistry*, John Wiley & sons, Great Britain, 1989.
- 11 G. Wettermark, in *Carbon-Nitrogen Double Bonds (1970)*, ed. S. Patai, John Wiley & Sons, Ltd., Chichester, UK, 1970, pp. 565–596.
- 12 R. N. Nurmukhametov, *Russ. Chem. Rev.*, 1967, **36**, 693–709.
- 13 R. Bonnett, *J. Chem. Soc.*, 1965, 2313–2318.
- 14 D. A. Nelson and J. J. Worman, *Tetrahedron Lett.*, 1966, **7**, 507–509.
- 15 N. Ebara, *Bull. Chem. Soc. Jpn.*, 1961, **34**, 1151–1158.
- 16 H. H. Jaffé, S.-J. Yeh and R. W. Gardner, *J. Mol. Spectrosc.*, 1958, **2**, 120–136.
- 17 A. Mehlhorn, J. Fabian and C. Perez, *J. Prakt. Chem.*, 1982, **324**, 267–278.
- 18 W. F. Smith, *Tetrahedron*, 1963, **19**, 445–454.
- 19 L. R. Knöpke, A. Spannenberg, A. Brückner and U. Bentrup, *Spectrochim. Acta, Part A*, 2012, **95**, 18–24.

- 20 Y. Luo, M. Utecht, J. Dokić, S. Korchak, H.-M. Vieth, R. Haag and P. Saalfrank, *ChemPhysChem*, 2011, **12**, 2311–2321.
- 21 M. Amati, C. Bonini, M. D'Auria, M. Funicello, F. Lelj and R. Racioppi, *J. Org. Chem.*, 2006, **71**, 7165–7179.
- 22 P. J. Orenski and W. D. Closson, *Tetrahedron Lett.*, 1967, **8**, 3629–3632.
- 23 B. V. Ioffe, O. V. Sverdlova and L. M. Korzhikova, *Theor. Exp. Chem.*, 1969, **3**, 64–66.
- 24 N. J. Turro, V. Ramamurthy and J. C. Scaiano, *Modern Molecular Photochemistry of Organic Molecules*, University Science Books, 2010; pp 705–800.
- 25 A. Padwa and F. Albrecht, *J. Org. Chem.*, 1974, **39**, 2361–2366.
- 26 D. Guha, A. Mandal, A. Koll, A. Filarowski and S. Mukherjee, *Spectrochim. Acta, Part A*, 2000, **56**, 2669–2677.
- 27 K. Kaur, S. Chaudhary, S. Singh and S. K. Mehta, *Sens. Actuators, B*, 2016, **232**, 396–401.
- 28 H. Ohta and K. Tokumaru, *Tetrahedron Lett.*, 1974, **15**, 2965–2968.
- 29 K. Rout, A. K. Manna, M. Sahu, J. Mondal, S. K. Singh and G. K. Patra, *RSC Adv.*, 2019, **9**, 25919–25931.
- 30 A. L. Berhanu, Gaurav, I. Mohiuddin, A. K. Malik, J. S. Aulakh, V. Kumar and K.-H. Kim, *TrAC, Trends Anal. Chem.*, 2019, **116**, 74–91.
- 31 R. Nakagaki, T. Kobayashi, J. Nakamura and S. Nagakura, *Bull. Chem. Soc. Jpn.*, 1977, **50**, 1909–1912.
- 32 M. Sliwa, N. Mouton, C. Ruckebusch, L. Poisson, A. Idrissi, S. Aloïse, L. Potier, J. Dubois, O. Poizat and G. Buntinx, *Photochem. Photobiol. Sci.*, 2010, **9**, 661–669.
- 33 J. M. Ortiz-Sánchez, R. Gelabert, M. Moreno and J. M. Lluch, *J. Chem. Phys.*, 2008, **129**, 214308.
- 34 Th. Arthen-Engeland, T. Bultmann, N. P. Ernsting, M. A. Rodriguez and W. Thiel, *Chem. Phys.*, 1992, **163**, 43–53.
- 35 P. Thirumurugan, D. Muralidharan and P. T. Perumal, *Dyes Pigm.*, 2009, **81**, 245–253.
- 36 H. Ö. Demir, T. Ağirgötüren, K. Meral, İ. Özyaytekin, A. Aygan, Ç. Küçükürkmen and M. Özhallaç, *J. Macromol. Sci. Part A Pure Appl. Chem*, 2013, **50**, 709–719.
- 37 A. Hantzsch, *Ber. Dtsch. Chem. Ges.*, 1890, **23**, 2325–2332.
- 38 R. Kuhn and H. M. Weitz, *Chem. Ber.*, 1953, **86**, 1199–1212.
- 39 E. Fischer and Y. Frei, *J. Chem. Phys.*, 1957, **27**, 808–809.
- 40 A. Padwa and F. Albrecht, *J. Am. Chem. Soc.*, 1972, **94**, 1000–1002.
- 41 A. Padwa and F. Albrecht, *Tetrahedron Lett.*, 1974, **15**, 1083–1086.
- 42 P. J. Coelho, M. C. R. Castro and M. M. M. Raposo, *J. Photochem. Photobiol., A*, 2013, **259**, 59–65.
- 43 D. G. Anderson and G. Wettermark, *J. Am. Chem. Soc.*, 1965, **87**, 1433–1438.
- 44 R. Potashnik and M. Ottolenghi, *Chem. Phys.*, 1969, **51**, 3671–3681.
- 45 A. Padwa and F. Albrecht, *J. Am. Chem. Soc.*, 1974, **96**, 4849–4857.
- 46 W. G. Herkstroeter, *J. Am. Chem. Soc.*, 1976, **98**, 330–336.
- 47 M. S. M. Rawat, S. Mal and P. Singh, *Open Chem. J.*, 2015, **2**, 7–19.
- 48 M. Irie, T. Fukaminato, K. Matsuda and S. Kobatake, *Chem. Rev.*, 2014, **114**, 12174–12277.
- 49 R. S. Becker and W. Frank. Richey, *J. Am. Chem. Soc.*, 1967, **89**, 1298–1302.
- 50 M. Jadhao, O. R. Meitei, R. Joshi, H. Kumar, C. Das and S. K. Ghosh, *J. Photochem. Photobiol., A*, 2016, **326**, 41–49.
- 51 E. S. Huyser, R. H. S. Wang and W. T. Short, *J. Org. Chem.*, 1968, **33**, 4323–4325.
- 52 B. Fraser-Reid, A. McLean and E. W. Usherwood, *Can. J. Chem.*, 1969, **47**, 4511–4514.
- 53 A. Padwa, W. Bergmark and D. Pashayan, *J. Am. Chem. Soc.*, 1969, **91**, 2653–2660.
- 54 J. M. Hornback, G. S. Proehl and I. J. Starner, *J. Org. Chem.*, 1975, **40**, 1077–1079.
- 55 T. H. Koch, R. J. Sluski and R. H. Moseley, *J. Am. Chem. Soc.*, 1973, **95**, 3957–3963.
- 56 N. Tushima and H. Hirai, *Tetrahedron Lett.*, 1970, **11**, 433–436.
- 57 R. L. Furey and R. O. Kan, *Tetrahedron*, 1968, **24**, 3085–3093.
- 58 B. Singh and E. F. Ullman, *J. Am. Chem. Soc.*, 1967, **89**, 6911–6916.
- 59 D. Sampedro, A. Soldevilla, M. A. Rodríguez, P. J. Campos and M. Olivucci, *J. Am. Chem. Soc.*, 2005, **127**, 441–448.
- 60 P. Beak and J. L. Miesel, *J. Am. Chem. Soc.*, 1967, **89**, 2375–2384.
- 61 M. Kojima and M. Maeda, *J. Chem. Soc. D*, 1970, 386–387.
- 62 D. Armesto, O. Caballero and U. Amador, *J. Am. Chem. Soc.*, 1997, **119**, 12659–12660.
- 63 D. Armesto, M. J. Ortiz, A. R. Agarrabeitia and M. Martin-Fontecha, *J. Am. Chem. Soc.*, 2001, **123**, 9920–9921.
- 64 R. T. Taylor, M. Douek and G. Just, *Tetrahedron Lett.*, 1966, **7**, 4143–4148.

- 65 G. Just and L. S. Ng, *Can. J. Chem.*, 1968, **46**, 3381–3389.
- 66 M. Cunningham, L. S. N. Lim and G. Just, *Can. J. Chem.*, 1971, **49**, 2891–2896.
- 67 H. Izawa, P. D. Mayo and T. Tabata, *Can. J. Chem.*, 1969, **47**, 51–62.
- 68 T. Sasaki and M. Takahashi, *Bull. Chem. Soc. Jpn.*, 1968, **41**, 1967–1968.
- 69 J. S. Babra, A. T. Russell, C. D. Smith and Y. Zhang, *Tetrahedron*, 2018, **74**, 5351–5357.
- 70 C. Lefebvre, C. Michelin, V. DjouEou Mvondo, T. Martzel, V. Bulach, M. Abe and N. Hoffmann, *J. Org. Chem.*, 2018, **83**, 1867–1875.
- 71 D. Staveness, J. L. Collins III, R. C. McAtee and C. R. J. Stephenson, *Angew. Chem. Int. Ed.*, 2019, **58**, 19000–19006.
- 72 O. A. Mukhina, N. N. Bhuvan Kumar, T. M. Arisco, R. A. Valiulin, G. A. Metzler and A. G. Kutateladze, *Angew. Chem. Int. Ed.*, 2011, **50**, 9423–9428.
- 73 N. S. Nandurkar, N. N. B. Kumar, O. A. Mukhina and A. G. Kutateladze, *ACS Comb. Sci.*, 2013, **15**, 73–76.
- 74 N. N. B. Kumar, O. A. Mukhina and A. G. Kutateladze, *J. Am. Chem. Soc.*, 2013, **135**, 9608–9611.
- 75 W. C. Cronk, O. A. Mukhina and A. G. Kutateladze, *J. Org. Chem.*, 2014, **79**, 1235–1246.
- 76 O. A. Mukhina, N. N. B. Kumar, T. M. Cowger and A. G. Kutateladze, *J. Org. Chem.*, 2014, **79**, 10956–10971.
- 77 O. A. Mukhina, D. M. Kuznetsov, T. M. Cowger and A. G. Kutateladze, *Angew. Chem. Int. Ed.*, 2015, **54**, 11516–11520.
- 78 W. J. Umstead, O. A. Mukhina, N. N. B. Kumar and A. G. Kutateladze, *Aust. J. Chem.*, 2015, **68**, 1672–1681.
- 79 N. N. B. Kumar, D. M. Kuznetsov and A. G. Kutateladze, *Org. Lett.*, 2015, **17**, 438–441.
- 80 W. J. Umstead, O. A. Mukhina and A. G. Kutateladze, *Eur. J. Org. Chem.*, 2015, **2015**, 2205–2213.
- 81 D. M. Kuznetsov, O. A. Mukhina and A. G. Kutateladze, *Angew. Chem. Int. Ed.*, 2016, **55**, 6988–6991.
- 82 D. M. Kuznetsov and A. G. Kutateladze, *J. Am. Chem. Soc.*, 2017, **139**, 16584–16590.
- 83 O. A. Mukhina, W. C. Cronk, N. N. B. Kumar, M. C. Sekhar, A. Samanta and A. G. Kutateladze, *J. Phys. Chem. A*, 2014, **118**, 10487–10496.
- 84 C.-L. Chen, Y.-T. Chen, A. P. Demchenko and P.-T. Chou, *Nat. Rev. Chem.*, 2018, **2**, 131–143.
- 85 T. Patra, P. Bellotti, F. Strieth-Kalthoff and F. Glorius, *Angew. Chem. Int. Ed.*, 2020, **59**, 3172–3177.
- 86 D. Leifert and A. Studer, *Angew. Chem. Int. Ed.*, 2020, **59**, 74–108.
- 87 K. L. Cabbage, A. J. Orr-Ewing and K. I. Booker-Milburn, *Angew. Chem. Int. Ed.*, 2009, **48**, 2514–2517.
- 88 E. Paternò and G. Chieffi, *Gazz. Chim. Ital.*, 1909, **39**, 341–361.
- 89 N. C. Yang, M. Nussim, M. J. Jorgenson and S. Murov, *Tetrahedron Lett.*, 1964, **5**, 3657–3664.
- 90 N.-Chu. Yang, R. L. Loeschen and Diane. Mitchell, *J. Am. Chem. Soc.*, 1967, **89**, 5465–5466.
- 91 M. Fréneau and N. Hoffmann, *J. Photochem. Photobiol., C*, 2017, **33**, 83–108.
- 92 O. Tsuge, M. Tashiro and K. Oe, *Tetrahedron Lett.*, 1968, **9**, 3971–3974.
- 93 O. Tsuge, K. Oe and M. Tashiro, *Tetrahedron*, 1973, **29**, 41–46.
- 94 T. H. Koch and K. H. Howard, *Tetrahedron Lett.*, 1972, **13**, 4035–4038.
- 95 K. A. Howard and T. H. Koch, *J. Am. Chem. Soc.*, 1975, **97**, 7288–7298.
- 96 J. A. Hyatt and J. S. Swenton, *J. Chem. Soc., Chem. Commun.*, 1972, 1144–1145.
- 97 J. S. Swenton and J. A. Hyatt, *J. Am. Chem. Soc.*, 1974, **96**, 4879–4885.
- 98 T. Kumagai, K. Shimizu, Y. Kawamura and T. Mukai, *Tetrahedron*, 1981, **37**, 3365–3376.
- 99 J. S. Swenton, J. A. Hyatt, J. M. Lisy and J. Clardy, *J. Am. Chem. Soc.*, 1974, **96**, 4885–4891.
- 100 R. M. Rodehorst and T. H. Koch, *J. Am. Chem. Soc.*, 1975, **97**, 7298–7304.
- 101 T. Nishio, *J. Org. Chem.*, 1984, **49**, 827–832.
- 102 S. Futamura, H. Ohta and Y. Kamiya, *Chem. Lett.*, 1980, **9**, 655–658.
- 103 S. Futamura, H. Ohta and Y. Kamiya, *Bull. Chem. Soc. Jpn.*, 1982, **55**, 2190–2194.
- 104 T. Kumagai, Y. Kawamura and T. Mukai, *Tetrahedron Lett.*, 1983, **24**, 2279–2282.
- 105 T. Kumagai, Y. Kawamura and T. Mukai, *Chem. Lett.*, 1983, **12**, 1357–1360.
- 106 D. Sampedro, *ChemPhysChem*, 2006, **7**, 2456–2459.
- 107 D. Sampedro, A. Soldevilla, P. J. Campos, R. Ruiz and M. A. Rodríguez, *J. Org. Chem.*, 2008, **73**, 8331–8336.
- 108 M. R. Becker, E. R. Wearing and C. S. Schindler, *Nat. Chem.*, 2020, **12**, 898–905.
- 109 E. Kumarasamy, S. K. Kandappa, R. Raghunathan, S. Jockusch and J. Sivaguru, *Angew. Chem. Int. Ed.*, 2017, **56**, 7056–7061.
- 110 M. R. Becker, A. D. Richardson and C. S. Schindler, *Nat. Commun.*, 2019, **10**, 5095–5095.
- 111 M. Zhu, X. Zhang, C. Zheng and S.-L. You, *ACS Catal.*, 2020, 12618–12626.

112 R. Sakamoto, T. Inada, S. Sakurai and K. Maruoka, *Org. Lett.*, 2016, **18**, 6252–6255.

**Table of Content Entry**